Distribution Category UC-63d

DESIGN OPTIMIZATION AND PERFORMANCE CHARACTERISTICS OF A PHOTOVOLTAIC MICROIRRIGATION SYSTEM FOR USE IN DEVELOPING COUNTRIES

R. W. Matlin

COO-4094-33

10 July 1979

Massachusetts Institute of Technology
Lincoln Laboratory
Lexington, Massachusetts 02173

DISCLAIMER

ABSTRACT

Tens of millions of the world's poorest farmers currently subsist on small farms below two hectares in size. The increasing cost of animal irrigation coupled with decreasing farm size and the lack of a utility grid or acceptable alternate power sources is causing interest in the use of solar photovoltaics for these very small (subkilowatt) water pumping systems. The attractive combinations of system components (array, pump, motor, storage and controls) have been identified and their interactions characterized in order to optimize overall system efficiency. Computer simulations as well as component tests were made of systems utilizing flat-plate and low-concentration arrays, direct-coupled and electronic-impedance-matching controls, fixed and incremental (once or twice a day) tracking, DC and AC motors, and positive-displacement, centrifugal and verticle turbine pumps. The results of these analyses and tests are presented, including water volume pumped as a function of time of day and year, for the locations of Orissa, India and Cairo, Egypt. Finally, a description and operational data are given for a prototype unit that was developed as a result of the previous analyses and tests.

TABLE OF CONTENTS

LIST OF FIGURES

1.0 INTRODUCTION AND BACKGROUND

The world is undergoing a major increase in population which is creating a concomitant need for major increases in food supply. In India, for example, the population will be close to 1.0 billion by the year 2000 and will require a minimum foodgrain production approaching 200-million tons per year compared to present annual production of about 120-million tons. Similar increases are also required for most of the other developing nations.

Fifty-million farmers currently subsist on small farms below two hectares in size located on good land in the rich alluvium of the valleys and deltas of the Nile, Euphrates, Indus and Ganges, Irrawaddy and Mekong. Most of these areas experience extended dry seasons during which a second crop could be grown if water were available. Over large portions of these areas, water is available at lifts between 1 and 5 meters.

Extensive efforts at supplying irrigation water to the larger farms have been made and, in fact, have been quite successful. In India, nearly six-million private wells (dug wells and tube wells) have been installed since 1950. The small farmer faces a much more difficult situation because of the small size and fragmented status of his land holdings. The increasing cost of animal-powered irrigation coupled with decreasing farm size and the lack of utility grids have created interest in developing a pumping system which could be of aid to these small farms.

The search for such a micropumping system has been pursued by many researchers through a variety of possibilities, each of which was eventually found to be inadequate, inappropriate or too costly. It now appears that small mobile electric pumps, powered by photovoltaic arrays, could begin to fulfill the requirements when array prices drop below the US$4-5/watt range.

This paper deals with the development of such a unit. The major components to be included in the design of a micropumping system were identified and their interactions characterized for optimal system efficiency. Computer simulations as well as component tests were made of systems using flat-plate and low-concentration arrays, direct-coupled and electronic-impedance-matching controls, fixed and incremental (once or twice a day) tracking, DC and AC

motors, and positive-displacement, centrifugal and verticle turbine pumps. The results of the analyses and tests are presented, including water volume pumped as a function of time of day and year for the locations of Orissa, India and Cairo, Egypt. Finally, a description and operational data are given for a prototype unit that was developed as a result of the previous analyses and tests. This prototype micropump (see Figure 1) contains an array of 240-watts (peak) capacity, will pump 6 meters^3/hour (26 US gallons/minute) from a 5-meter head at full insolation and a 40°C ambient air temperature, includes the use of a maximum-power-point tracker and is mounted on a wheelbarrow frame for mobility.

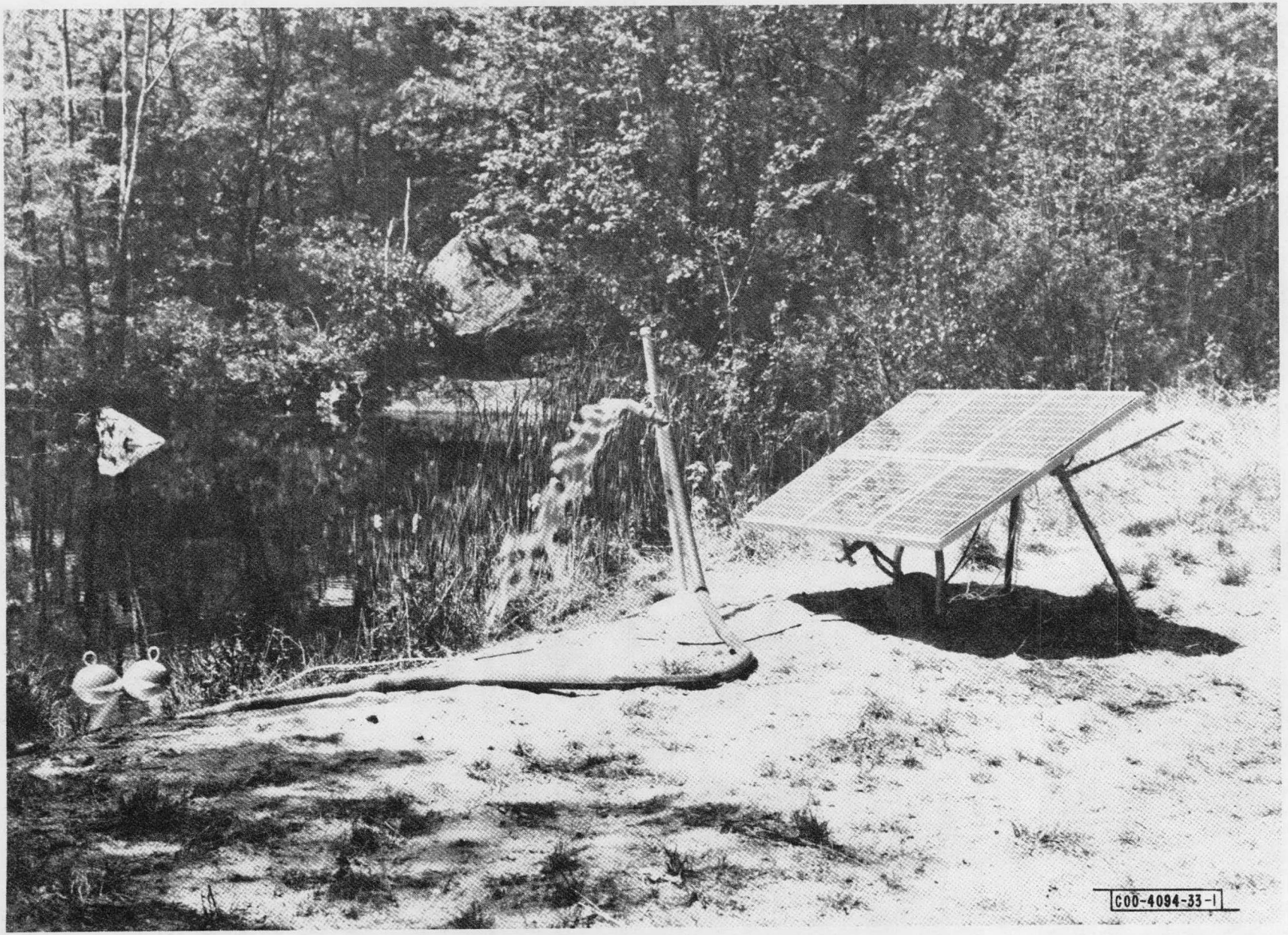

Figure 1 Prototype micropump.

2.0 CHOICE OF SYSTEM COMPONENTS

2.1 Pumps

2.1.1 Summary

There is a plethora of water pumps but for practical purposes only a few types are suitable for use in low-head microirrigation systems. Several types of pumps were considered for this application and are discussed below. A vertical turbine centrifugal pump was selected as best meeting the overall system needs.

2.1.2 Positive-Displacement Rotary Pumps

There are many kinds of positive-displacement rotary pumps: gas, screw, vane, lobe, piston, cam and a few other offshoots. The current-voltage (I-V) relationship for a motor coupled to a pump of this class is presented in Figure 2. The current demanded by the pump motor is essentially determined by the operating head while the pump rotational speed (and hence flow rate) is directly proportional to motor voltage. Hence, at a fixed head, the motor power demand is approximately proportional to pump flow rate. This characteristic is attractive since such a pump operated in conjunction with a solar array could exhibit a pump flow rate which varied directly with insolation level. However, to realize this pump-flow-rate/insolation-level relationship would require an electronic matching device (such as the maximum-power-point tracker described elsewhere in this report), because the motor/pump load is grossly mismatched to the solar-array power source.

Were this mismatch the only problem, the positive-displacement rotary pump would be worthy of consideration for this application. However, a second and much more serious problem is that these pumps cannot handle liquids containing grit or abrasive material. Pumping action relies on the close meshing of rotating elements, such as gears, lobes, vanes or screws, and on the close clearance between these parts and the pump casing. Generally the action is to trap small pockets of fluids between rotor and casing and transfer them from inlet to outlet. Any abrasive particles in the fluid will destroy the close tolerance between the mating parts, impair the pump's performance,

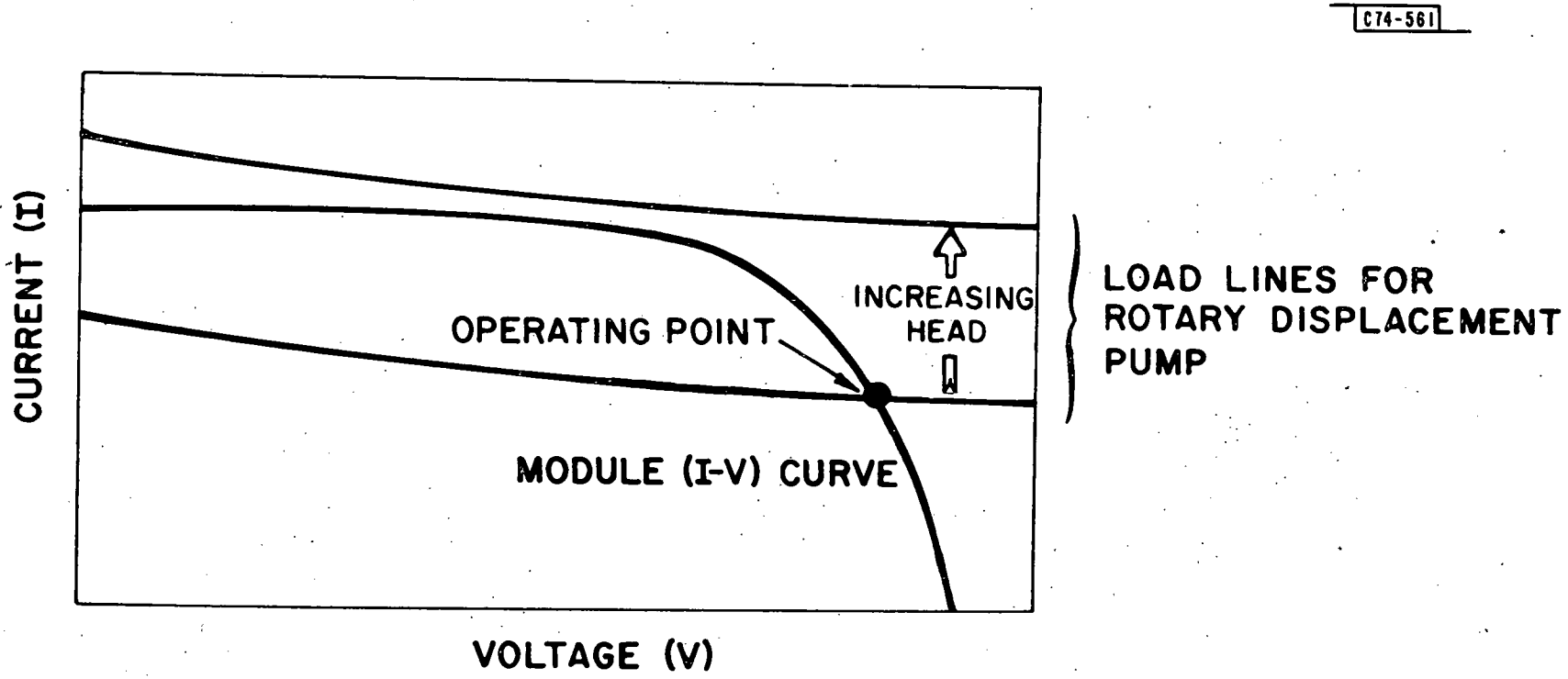

Figure 2 Current-voltage relationship.

and greatly decrease its efficiency. Water from wells, canals, rivers and lakes will very likely contain abrasive silt and sand; filtration to the level required for these pumps is impractical.

Finally, these pumps cannot operate against a closed discharge, and cannot run dry as they will be damaged. In summary, positive-displacement rotary pumps are unsuitable for microirrigation application.

2.1.3 Positive-Displacement Reciprocating Pumps

In the reciprocating positive-displacement pump, the pumping element may be a plunger, a piston or a pulsating diaphragm. The principle of the piston pump is this: a stroke in one direction causes a volume of liquid almost equal to the swept volume to be drawn through a valve into the cylinder, while movement of the piston in the reverse direction forces this pocket of liquid through another valve into the discharge line. A plunger is used in place of the piston at higher pressures. The diaphragm pump can be looked upon as a piston pump in which the piston has been replaced by a pulsating diaphragm.

Most displacement pumps are of the reciprocating type and are used extensively for water pumping in many locations in the world. They retain the advantages of rotary positive-displacement pumps, e.g., flow rate and efficiency are functions of speed alone and, hence, the head demanded does not influence performance. Like rotary pumps, power demand versus flow rate for reciprocating pumps is quasi-linear, but would require electronic circuitry for satisfactory operation from a solar array.

Reciprocating pumps do, however, have a number of disadvantages which make them undesirable for low-head micropumping applications. The discharge characteristic of a reciprocating pump is a pulsating one. In small sizes these pumps are generally single-cylinder units with a flow rate which varies as a sine curve from zero at the point when the piston reverses its direction to a maximum when the piston is approximately halfway through its forward stroke. In addition, the pumping rate remains zero for the time it takes to fill the cylinder with liquid. In larger pumps, these pulsations can be reduced by the use of two (duplex) three (triplex) and even more cylinders. They can be smoothed further by use of double-acting cylinders which incorporate suction

and discharge valves at both ends of the cylinder. But for units small and inexpensive enough to use in micropumping applications, only one piston would be utilized. Since a photovoltaic array continuously provides power and a reciprocating pump draws a sinusoidally varying power, some intermediate energy storage is mandated. In principle, such storage could be in inductive or capacitive elements (electrical), in batteries (chemical), or in a flywheel (mechanical). Inductive or capacitive storage is impractical because of the physical size of the storage elements. The use of batteries in these remote, mobile units is undesirable, as discussed in Section 2.5. The addition of a flywheel onto a pump that already tends to be heavy, bulky and long, also seems to be undesirable for this application.

An additional problem caused by the characteristic torque and power input varying directly with head is that these pumps must exert full-load torque in starting. This requires very heavy starting currents.

Piston and plunger pumps are ordinarily designed to operate at piston speeds of 15 cm/sec for pumps of 15-cm stroke or less to 40 or 45 cm/sec for pumps of 40-cm stroke or over. These low piston speeds require, in turn, extremely low shaft speeds, as compared with ordinary motor speeds. This condition is usually met by installing a slow-speed motor with a belt or chain drive, by a double-gear reduction, or by a combination of the two. This reduction in speed necessarily involves a considerable loss of power, and this loss must be considered in comparing pump efficiencies. Also low-speed motors tend to be bigger, heavier and less efficient than higher-speed motors.

Although reciprocating pumps can handle fluids containing some contamination, the seals are subject to wear and valves may stick open or leak because of trapped particles between the valve and valve seat.

Finally, for piston pumps it should be noted that the efficiency at low depths is degraded by the friction of the seal; it becomes more suitable at increasing depths.

In summary, these units are heavy, have a pulsating discharge and power requirement, cannot operate against a closed discharge, are complicated by the use of valves, have frictional surfaces, require low shaft speeds, and tend to be much more expensive than centrifugal pumps in small sizes.

2.1.4 Centrifugal Pumps

Centrifugal pumps, as their name implies, use centrifugal force to transfer liquids from one pressure to a higher pressure. Liquid enters the centrifugal pump at the center of a rotating impeller, imparting energy to the liquid. The centrifugal force discharges the liquid through a volute of diffuser blades.

A centrifugal pump at a particular speed will deliver any capacity from zero to its corresponding maximum value, depending on the pump's size, design and suction condition. The total head developed, the power to drive the pump and the resulting efficiency vary non-linearly with capacity. The manner in which head varies with capacity at constant speed is called the pump characteristic. A typical relationship between head, capacity, efficiency and power for a centrifugal pump is shown in Figure 3. The graph demonstrates that as capacity increases, the total head the pump is able to develop is reduced. This is quite different from the positive-displacement pumps described in the previous sections.

The power to drive a pump is proportional to the delivered flow and developed head. For a centrifugal pump the delivered flow varies directly with the impeller speed, while the developed head varies as the square of the impeller speed. Thus the power to drive this type of pump varies as the third power of the speed. Since the motor speed is directly proportional to the input voltage, centrifugal pumps have a current-voltage (I-V) characteristic which could work moderately well with direct connection to a photovoltaic array, as seen in Figure 4. However, for reasons which will be presented later, electronic circuitry to match the pump/motor to the solar array is still desirable.

The efficiency of centrifugal pumps can be high and in well-designed pumps shows very little dropping off after comparatively long service. In order to determine what efficiencies can be expected in centrifugal pumps under different demands of head, capacity and speed, many pumps have been tested and the resulting data presented graphically in treatises on pumps. A recently updated graph showing this information is shown in Figure 5. Efficiency is shown as a function of specific speed and flow rate. The specific speed applicable to micropumping systems is in the 2500 to 3000 range for lifts of 3 to 5 meters. Thus for flow outputs of from 30 to 50 gpm, peak efficiencies of from 60 to 65%

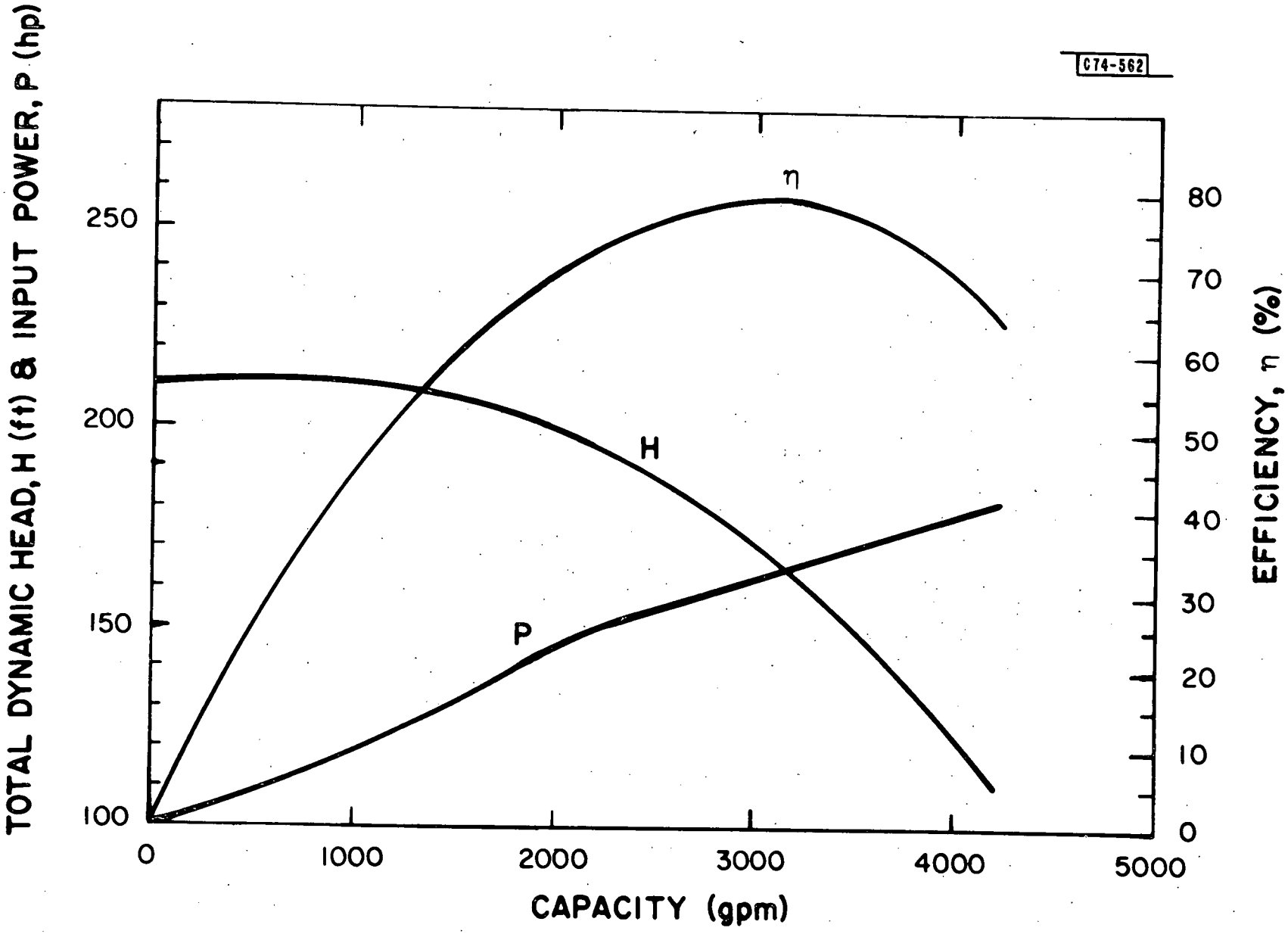

Figure 3 Centrifugal pump efficiency relationships.

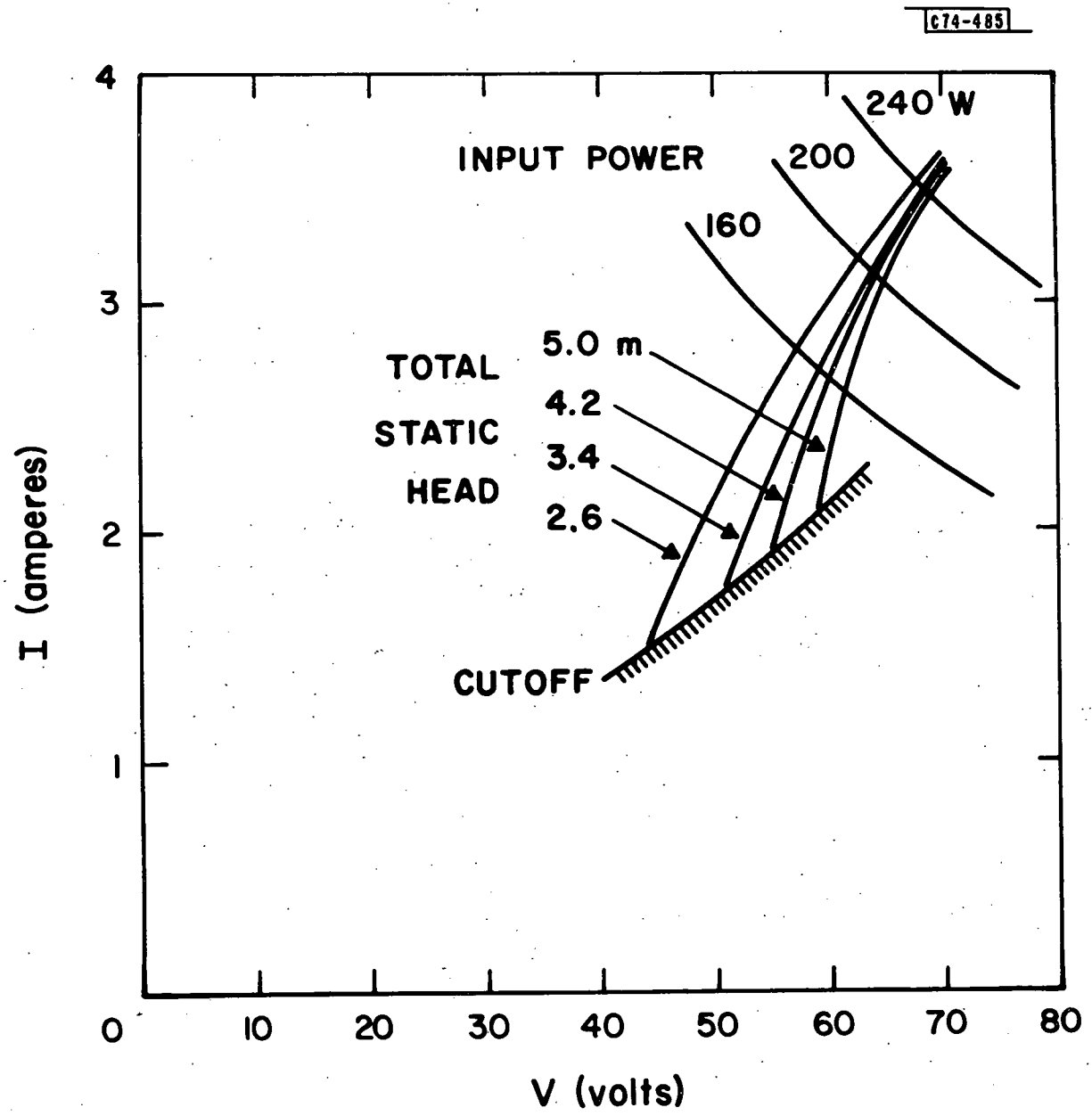

Figure 4 Pump set I-V load curves for different total static heads.

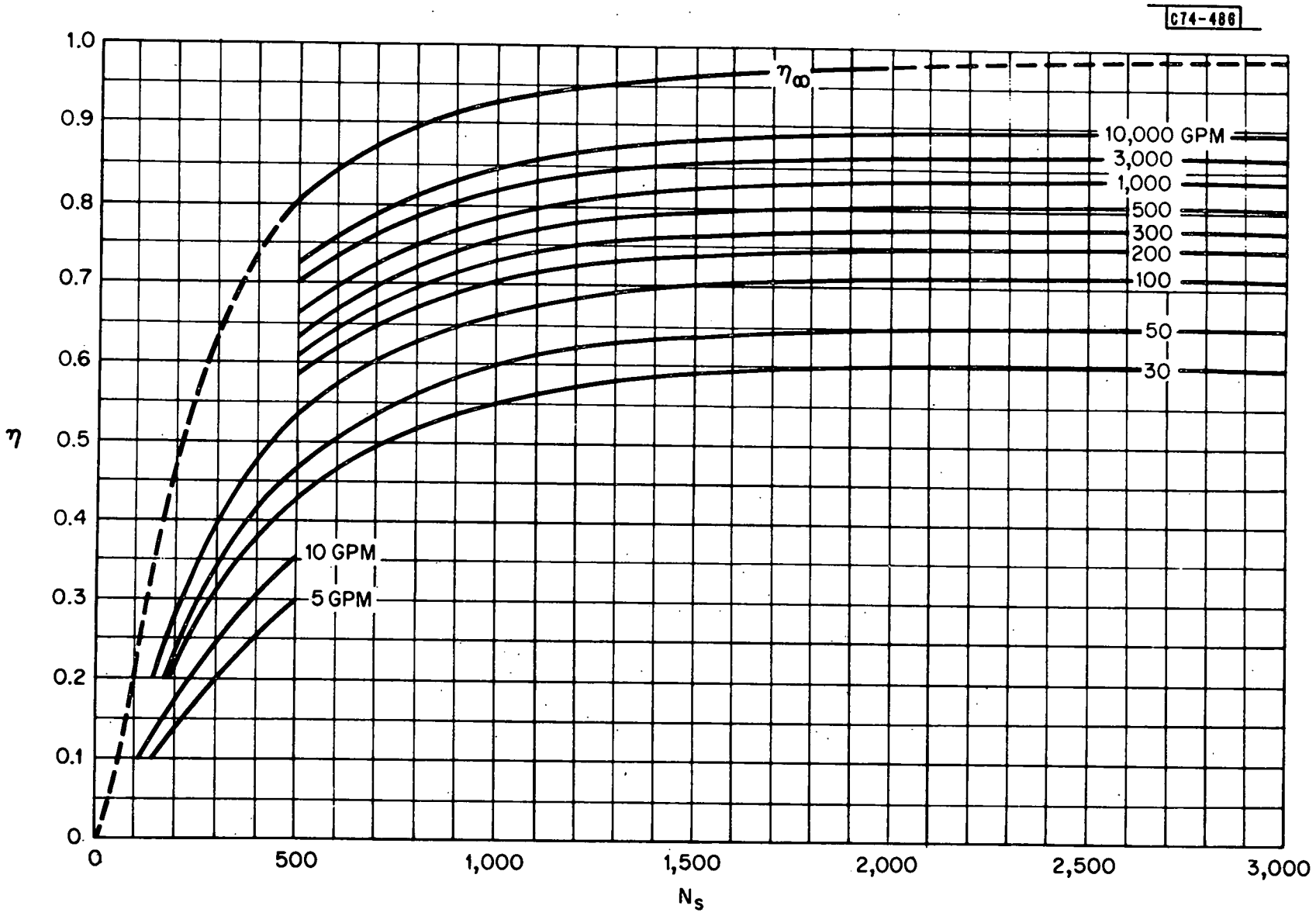

*specific speed = $N_S = \frac{n\sqrt{Q}}{H^{3/4}}$

where n = rpm H = head (feet)

Q = flow (gallons/min.)

Figure 5 Efficiency as a function of specific speed* and capacity.

should be expected. A pump efficiency will rise from zero to this peak value and then fall again; when specific speed is low (< 3000), the curve is relatively flat at its maximum, whereas at high specific speed (> 8000) it shows a narrower plateau. This characteristic (efficiency varying with head) brings about a need for different impellers, and possibly different pump housings for micropumping units used in widely varying situations, i.e., 1-meter canal lifts versus 3- to 5-meter dug-well or tube-well lifts.

One of the fundamental factors in the relative performance of displacement pumps and centrifugal pumps is that the former are capable of creating a partial vacuum in the suction connection while the latter are not. Therefore, a centrifugal pump installed above the source of supply must be primed before starting, i.e., the suction piping and the pump casing must be filled with liquid, and all air expelled. Placing the pump on the surface and using a foot valve to maintain prime is a well known and widely used technique. However, this technique generally requires an attendant when the motor is activated so that the pump can be reprimed if the foot valve has not functioned properly. A person, however, will not always be in attendance during activation of a photovoltaically powered pump. Clouds will periodically shut down the system during the day, with the system automatically reactivating unattended. However, should the foot valve fail unobserved, the pump would run dry. It is therefore believed that a submersed pump would best solve this problem. For a small mobile micropumping unit, the use of a close-coupled submersible motor would be required.

2.2 Motors

2.2.1 Motor Consideration

For proper selection of a pump motor, it is useful to understand the load requirements which the pump imposes on the motor. Figure 6 illustrates the flow rate and torque load as a function of speed under two different heads for a typical centrifugal pump employed in this project. The maximum flow rates plotted for each head correspond approximately to the maximum pump system capability using a 240-watt array. Significant characteristics of these curves are:

1. Maximum operating speed is between 3000 and 4000 rpm. Speeds much greater will probably shorten motor and pump bearing life.
2. Under load, motor speed can vary from 15 to 30 percent, depending on available power from the solar array.
3. Starting torque is not a problem. The pump must attain sufficient speed to overcome the head back pressure. Below this speed, the pump impeller slip with no flow produces only a negligible torque requirement.

Changing the pump impeller to provide more efficient operation at different heads would change the threshold speed, but the basic characteristics noted would still apply.

Additional motor characteristics to be considered are efficiency, maintenance requirements, reliability and horsepower. Efficiency is of the utmost importance in minimizing the required solar array size, as can be seen from Figure 7. Maintenance and reliability may not be important factors in a laboratory environment or when a nearby service shop is available, but in remote areas and extreme environments they assume major significance.

Horsepower requirements are dictated by the solar-array size, if one assumes relatively small losses between the array output and motor input. A given motor will have a manufacturer's horsepower rating stamped on the nameplate, but this is by no means a hard and fast limitation. The two prime concerns are internal operating temperature and brush currents (if the motor has brushes). Most motors are rated at some internal temperature rise under steady-state full load; operation at higher temperatures is liable to degrade insulation and lead to

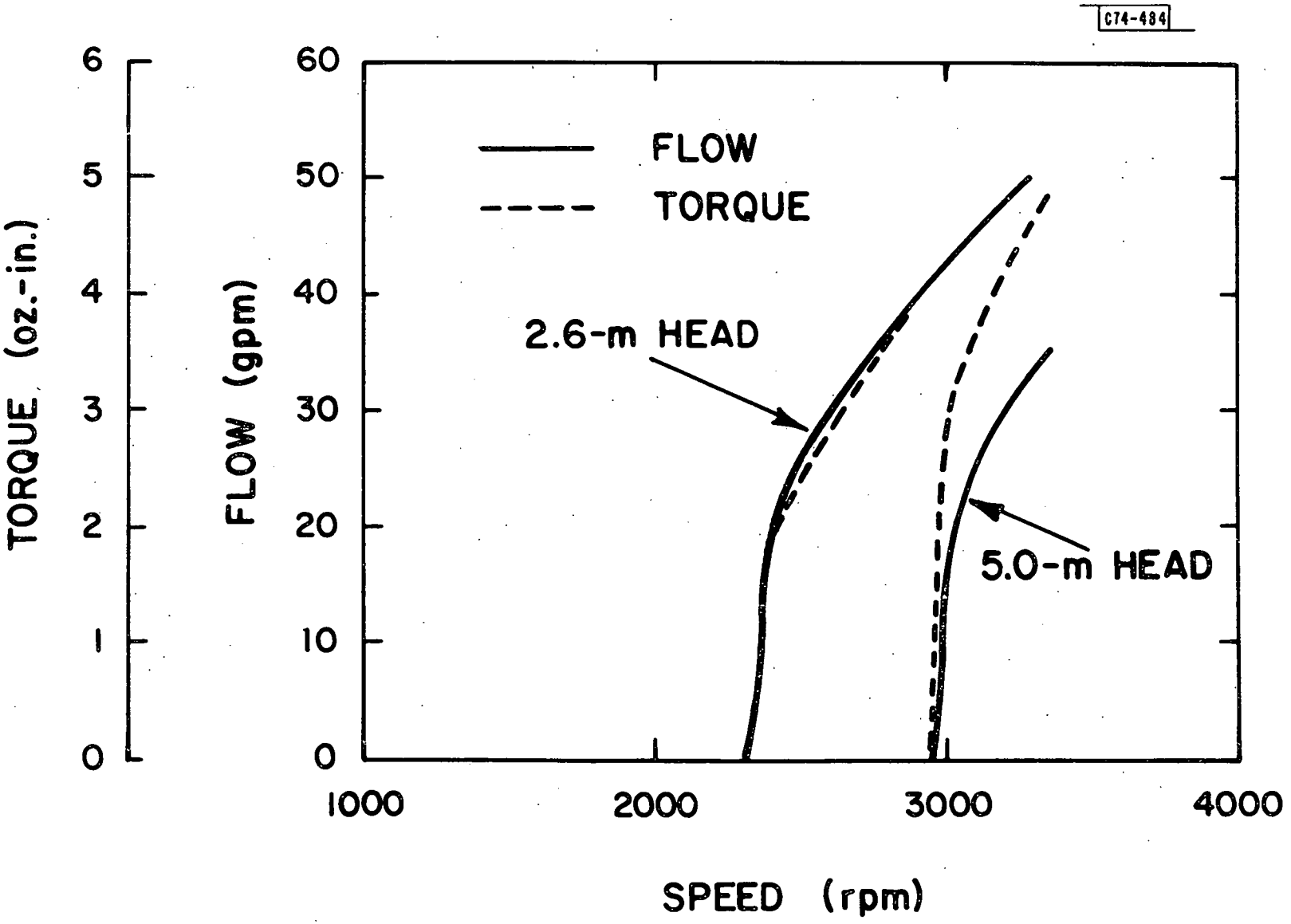

Figure 6 Pump flow rate and torque vs. speed.

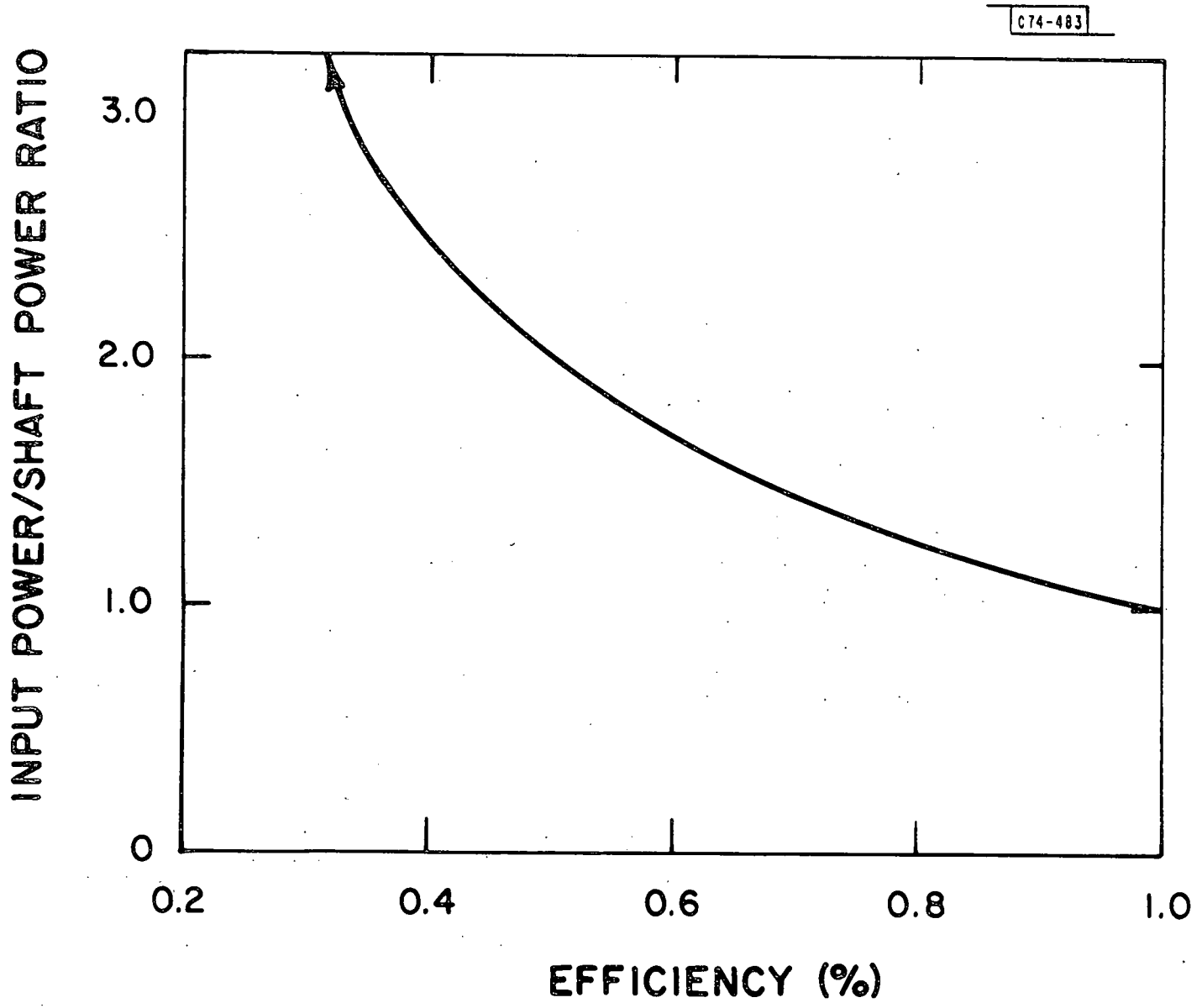

Figure 7 Normalized motor input power vs. efficiency.

winding short circuits. Brush currents must be kept below some maximum value; if currents exceed this value, brush arcing is likely to occur, causing rapid deterioration of the brushes and possible commutator damage. However, as long as the motor can be maintained within these limits, operation in excess of the manufacturer's rating is quite feasible.

2.2.2 Choice of Motor

The motor selected for this application is a 1/3-hp DC permanent magnet motor specially wound to deliver rated load at 3000 rpm when operating at 60 V. Efficiency is 85% under these conditions and holds up very well over a considerable range of operating conditions, as can be seen from the data plotted in Figure 8. Since the motor coupled to the pump is operated as a sealed underwater unit, case temperature of the assembly is maintained at the water ambient, permitting operation above rated power if additional power is available from the array.

Some other features which make DC permanent magnet motors attractive are: lighter weight, smaller size, greater reliability (since there is no field winding to fail), lower cost (windings are expensive to manufacture), and operation over a very wide range of input voltages.

Other types of motors were considered initially, but all fell short when compared with the DC permanent magnet motor. Table I summarizes efficiency data computed from manufacturers' data for a large number of motors in the 1/4-1/3 hp range. As can be seen from the tabulated efficiencies, all AC motors plus AC/DC universal motors exhibit inferior performance when compared with the DC permanent magnet motor. For larger installations, 3-phase motors and capacitor-start/induction-run motors perform quite efficiently (e.g., 64% efficiency at 2 hp, 72% efficiency at 10 hp, and 78% efficiency at 50 hp), but they cannot compete in the fractional-horsepower range.

Another problem with any AC motor (except AC/DC universal motors) is the requirement to run at close to synchronous speed. To operate an AC motor from a solar array requires a DC-to-AC converter; speed variations of 15-30 percent require that the AC frequency be varied. It is possible to design electronic

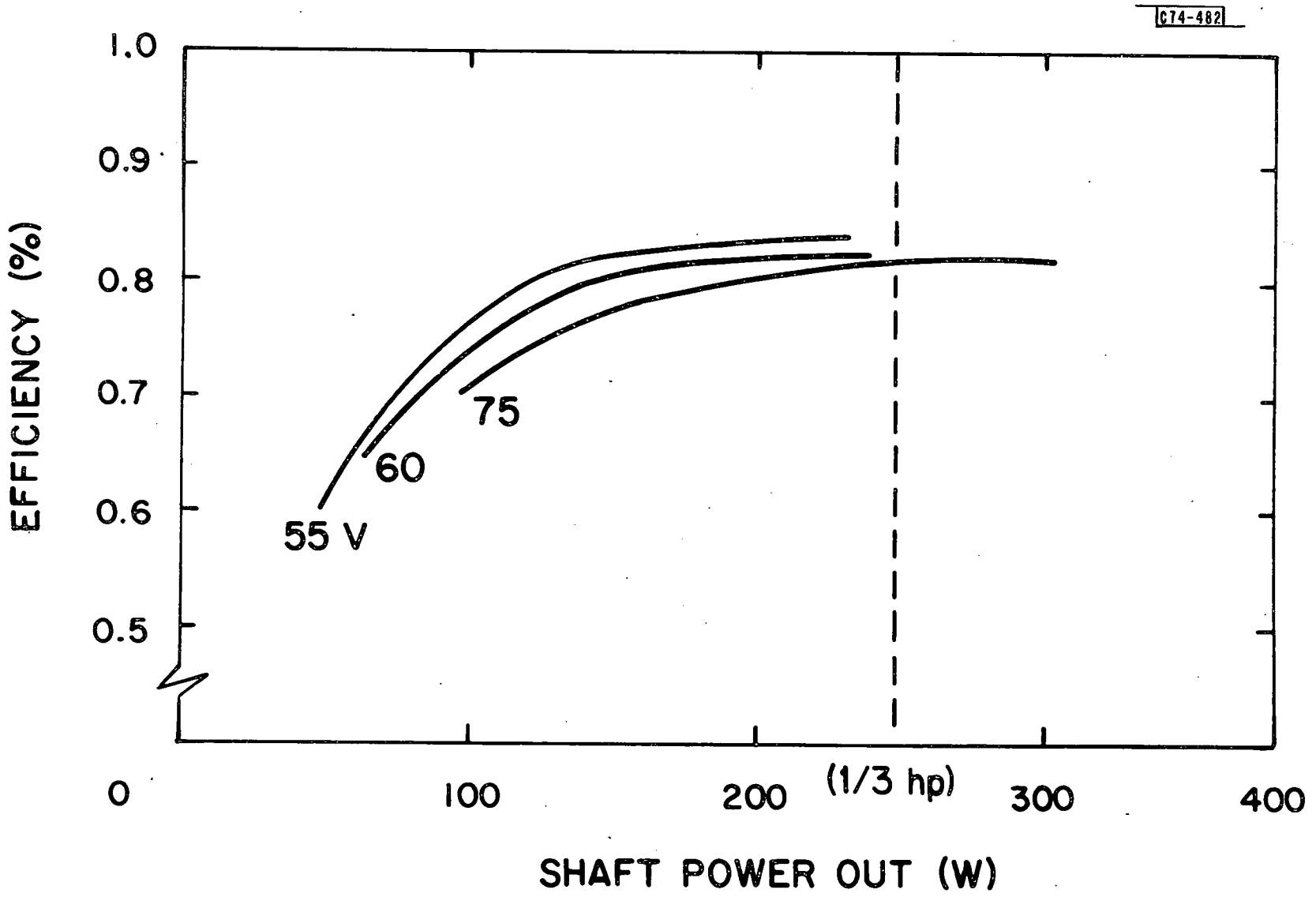

Figure 8 Motor efficiency vs. output power.

control systems to accomplish these functions, but at this power level the circuit complexities and efficiency losses would be unwarranted even if highly efficient motor designs were available.

Series and shunt wound DC motors were also considered and discarded. Both are less efficient than the DC permanent motor. Series motors can also run away when unloaded, often to the point of self-destruction--a very real possibility if a farmer pulls his pump set out of the water without turning off the power switch.

TABLE 1

MOTOR EFFICIENCIES (1/4 to 1/3 HP)

Motor Type	Efficiency
AC Induction - Shaded Pole	19% - 24%
- Capacitor Start/Induction Run	23% - 43%
- Split Phase	27% - 46%
- 3 Phase	35% - 50%
- Permanent Split Capacitor	28% - 64%
AC/DC Universal	46% - 51%
DC Permanent Magnet	69% - 86%

2.3 Maximum-Power-Point Tracker

Maximum-power-point tracking or optimization systems can be designed using either source or load characteristics as control variables. Since maximum power criteria depend not only on static operating points but also on derivatives at these operating points, a maximum-power-point tracker can never operate statically at a maximum power point, but must always vary slightly around the operating point. Several maximum-power-point trackers have been developed and described in the literature. Nearly all maximize power from the source, making use of the criteria (see Appendix A):

$$\frac{dI}{dV} = -\frac{I}{V}$$

All such systems suffer from one or more of the following:

1) Four variables (V, I, dV, dI) must be monitored at the source;
2) Multiplication of variables must be performed;
3) An approximation or estimation of $\frac{dI}{dV}$ is employed;
4) Maximum source power may not correspond to maximum load power if source-to-load conversion efficiency varies with changing-source operating point.

Recently, Landsman (MIT/Lincoln Laboratory Report C00/4094-17) has developed a simple maximum-power-point tracker which bypasses most of the above objections. This system can be designed to work with any load type described in the Appendix, provided that load-power plotted versus the single-valued variable does not reach a maximum. Within this constraint, the technique relies on the observation that a change in the single-valued variable (in this case voltage applied to the load) has the same sign as the corresponding change in load power.

A simplified block diagram of the maximum-power-point tracker is shown in Figure 9. For this pumping application, the array and the pump motor are designed so that the array-maximum-power operating voltage is always greater than the pump-motor voltage at that power output. This permits utilization of a high-efficiency pulsewidth-modulated down-converter (PWMDC) to match the array operating point to the pump-motor demand. Voltage input to the motor is monitored by means of a voltage-controlled oscillator (VCO), the output frequency of which is proportional to the voltage. Duty cycle of the PWMDC is

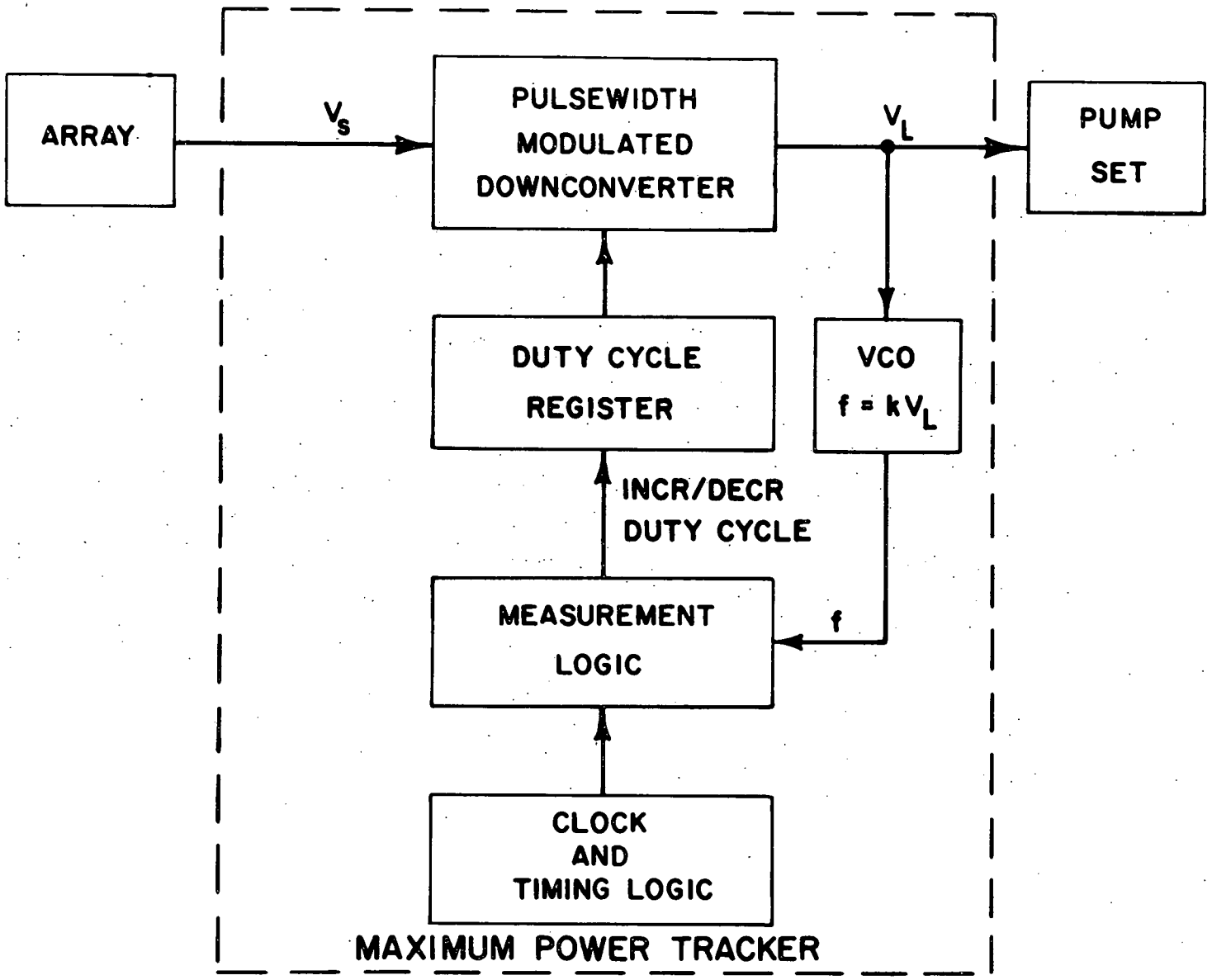

Figure 9 Maximum-power-point tracker block diagram.

controlled from the duty cycle register (DCR), which is periodically incremented or decremented by the measurement logic (ML). The clock and timing logic (CTL) provide time intervals and clock pulses for the measurement logic.

The maximization algorithm incorporated in the ML is shown in Figure 10. The algorithm cycle begins by resetting an up/down counter in the ML to zero. The counter is then set to COUNT DOWN and VCO pulses of frequency, f_d, are gated into the COUNT input for time period, T_d, determined by the CTL. Following this, the DCR is either incremented or decremented, depending on the logic state of an increment/decrement steering flipflop. The CTL inhibits further action for period T_s to permit the output voltage to settle to its new value. Next, the counter is set to COUNT UP, and VCO pulses of frequency, f_u, are gated into the COUNT input for period T_u (which is identical to T_d). At the end of T_u, the counter content is tested to determine what happened during the cycle. Consider these three cases:

1. Content > 0, $f_u > f_d$, power into load increased.
2. Content $= 0$, $f_u = f_d$, power into load remained constant.
3. Content < 0, $f_u < f_d$, power into load decreased.

For case 1 or 2, the load power increased or remained constant, so the algorithm cycle is considered complete and a new cycle initiated. For case 3, however, the load power decreased, which means that the DCR change was in the wrong direction. To correct this, the steering flipflop is complemented to its opposite state, after which a new cycle is initiated.

One can see from the description that the duty cycle will fluctuate up and down at the power maximizing point. In a practical maximum-power-point tracker which has been under test for several months at MIT/Lincoln Laboratory, the measured power ripple from this fluctuation is less than 1%. Overall efficiency of this unit, including all control circuit power, has been between 93% and 96.5%, depending on input and output operating points. In a demonstration system, the tracker has been used to couple a 240-watt six-module array to a pump set driven by a 1/3-hp DC permanent magnet motor. The array is configured for a V_{pmax} of 90 V at 1-kW/m^2 AMO illumination and 25°C array temperature. The motor is wound to operate at 60-V nominal input at rated horsepower and speed. Testing has

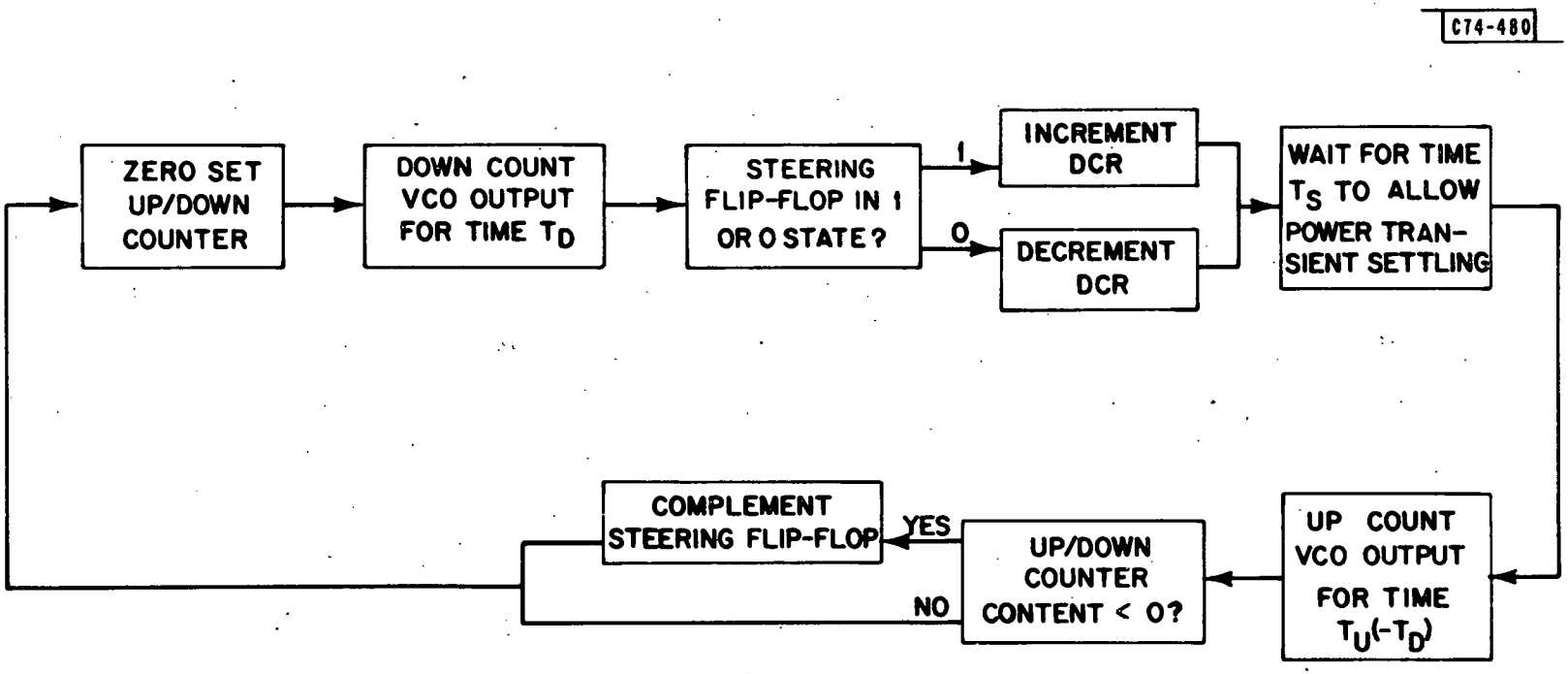

Figure 10 Power-maximization algorithm.

covered a wide range of array illumination and ambient temperatures and pumping loads. No instabilities or anomalous performance have been observed in the maximum-power-point tracker during this test period.

2.3.1 Maximum-Power-Point Tracker Benefits

Recently a computer simulation was used to compare pump system operation throughout the year with and without a maximum-power-point tracker. Insolation data werebased on estimates for Orissa, India. Pumping heads were assumed to vary seasonally from 1.0 m to 4.5 m. Parameters for the solar array, the pump motor and the pump were selected to optimize the overall annual performance without the maximum-power-point tracker. The simulator results showed that, despite the 4 to 7% power loss in the maximum-power-point tracker, the total quantity of water pumped during the year was about 7% greater with the maximum-power-point tracking system.

The important point to note is not that operation without a maximum-power-point tracker was only 7% less efficient but that the system parameters with no maximum-power-point tracker had to be carefully matched to the site parameters to achieve that performance. Lack of optimization to the specific pumping situation will lessen performance even more. Computer-optimized parameters for each site have been advocated by one group studying this problem on the grounds that inclusion of electronics and/or batteries compromises reliable operation in remote environs. Such optimization may be viable if only a few installations are being considered but, if one is considering thousands of such installations, the field engineering costs not to mention manufacturing costs, become enormous. Also, proper manufacturing techniques and production testing can lead to quite reliable electronic systems.

With the maximum-power-point tracker included, matching the system to the site should not be necessary. A standard pumping system can be used under significantly different conditions and still function optimally. Consider the data shown in Figure 11 for direct connection of a pump system to a 240-watt array. The array I-V characteristic is shown for 100% and 25% insolation values and for three different temperatures which can realistically occur under field operating conditions. For insolation values between these shown, the maximum-power-point

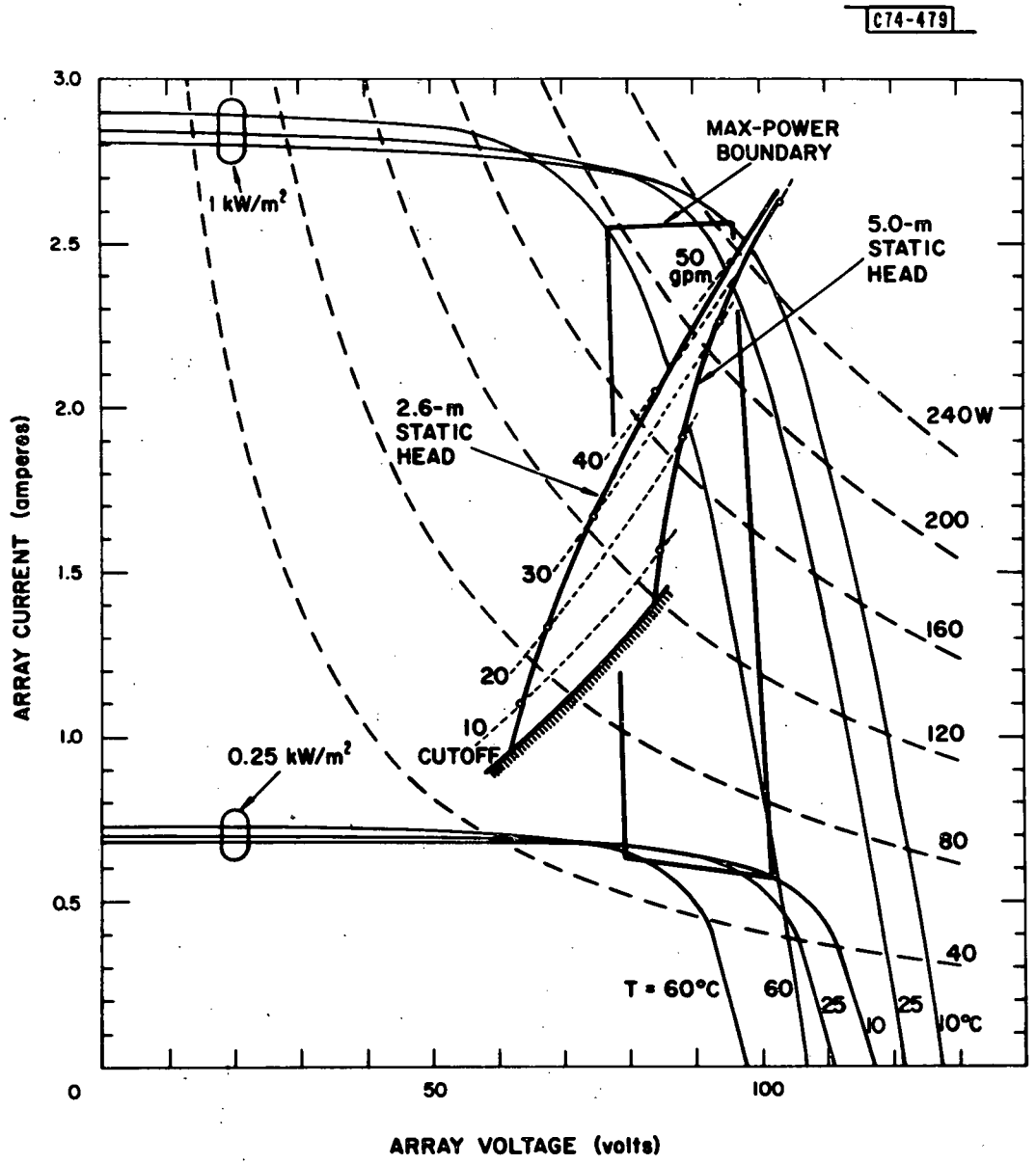

Figure 11 Pumping capability for pump directly connected to array.

of the array will fall within the heavily outlined boundary. Pump motor data has been scaled to assume near-optimum operation under 100% insolation with the array at 25°C.

It is apparent that this system will have poor efficiency for varying insolation and array temperature compared with what is possible with a maximum-power-point tracker. Consider two examples: (1) A 33% insolation 10°C array characteristic (representative of early morning) would just reach threshold against the 2.6-m head shown in Figure 11, yet with a maximum-power-point tracker the system would pump 3.4 m^3/hour (15 gpm)! (The reader can verify this by scaling 25% 10°C curve by one-third in current.) (2) The 100% insolation 60°C is representative of the array at high noon. Against a 5-m head the system will pump about 5 m^3/hour (22 gpm); power maximizing increases this to about 6 m^3/hour (26 gpm).

Drastically different field conditions may require pump or motor modifications. Different impeller designs may be required for pumping against very high or low heads. In areas where insolation is low for long periods because of overcast skies, it may be necessary to choose a pump design which maintains reasonable efficiency at low flow rates or to enlarge the solar array. In such circumstances, a basis of site data is obviously needed to make intelligent design changes, but the data requirements are minimized when the maximum-power-point tracker is used.

2.4 Concentrator Systems

The use of reflecting surfaces to concentrate solar radiation, and thereby decrease the number of photovoltaic cells required, has attracted attention among many photovoltaic researchers because of the high cost of solar cells. As the cost of solar cells declines, however, this approach begins to lose appeal. An investigation into the attractiveness of concentrators with micro-pumping units was made. A comparison of the advantages and disadvantages led to the decision to use flat-panel non-concentrating arrays with the small pumping units.

Concentrators may be constructed in several different ways by using refractive optics (usually Fresnel) or reflective optics (mirrored surfaces), which may be linear (trough types) or circular (parabolas, cones, etc.). Systems can track in two axes or one axis, be seasonally adjusted, or be stationary. In general, any system employing concentration ratios over ten requires two-axis tracking mechanisms to be effective. Tracking mechanisms of this type are uneconomical when used with such small systems and are unsuitable for use in remote areas which lack repair facilities. Also, systems employing concentration ratios of less than ten may still need tracking, depending on the particular configuration under investigation. For micro-pumping applications, the most suitable configuration appears to be a trough-type linear concentrator, using reflective optics with a geometric concentration ratio of approximately three.

Simulations and experiments were carried out using a concentrator of the type described to determine the overall performance of such a system. Several problems with these systems were identified and investigated. One problem is degradation in performance as the sun's path diverges from the meridian plane of the collector. Figures 12a and 12b show the sun's daily path along a trough-type concentrator. Except at the equinoxes, the sun's path describes an arc compared to an untracked concentrator's major axis. This can be expressed as an off-axis angle, θ, between the sun and the collector which causes performance degradation. This angle, θ, is shown as a function of time of day and month of year in Figures 13 and 14. The effect of this off-axis angle on a typical

C74-469

Motion Of Sun Relative To Array Location

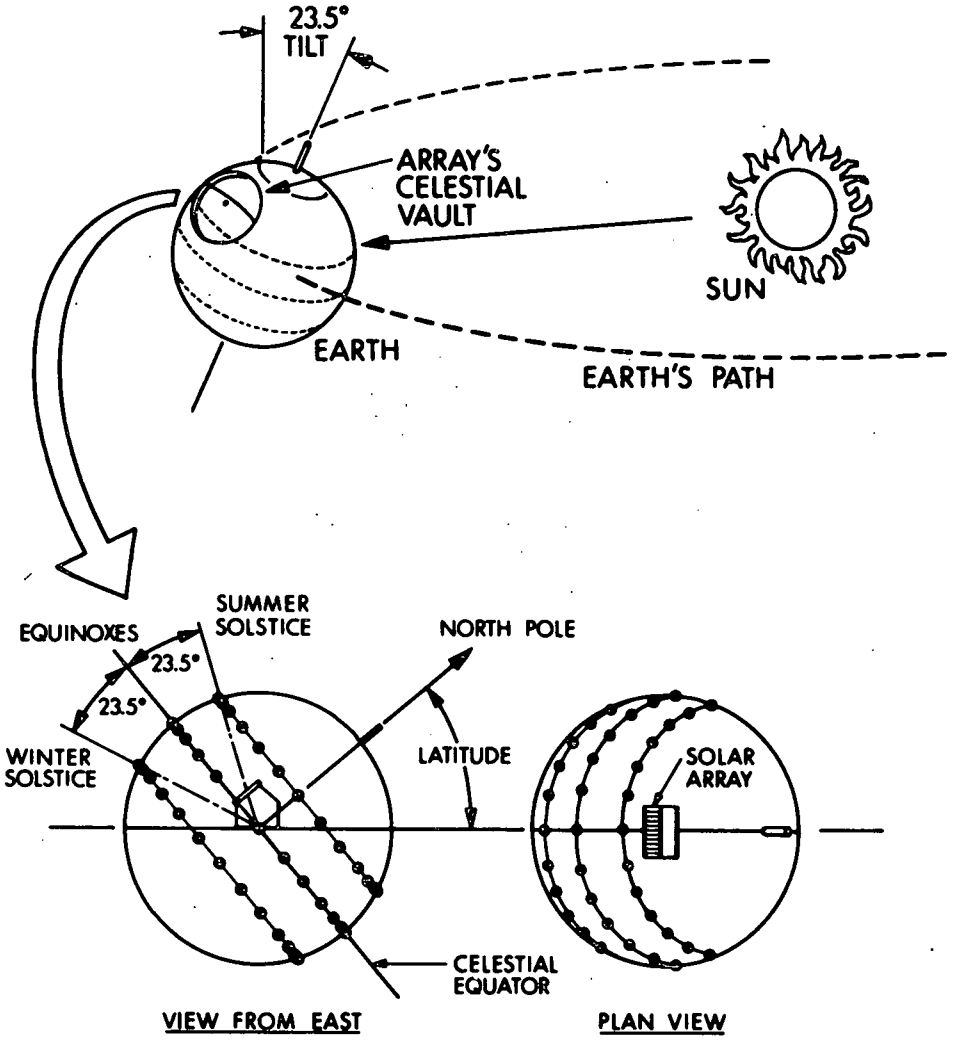

ARRAYS CELESTIAL VAULT

Figure 12a

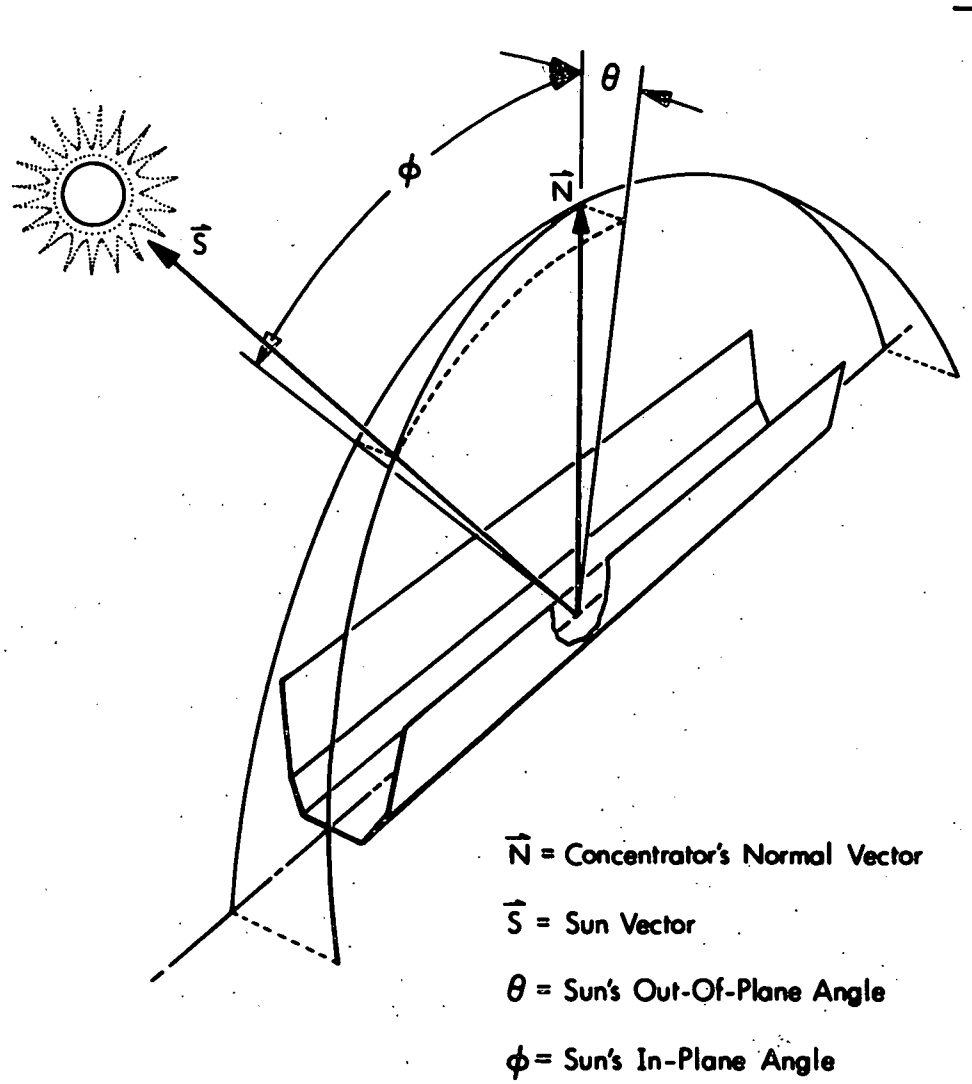

SUN'S PATH RELATIVE TO A
LINE-FOCUS CONCENTRATING COLLECTOR

Figure 12b

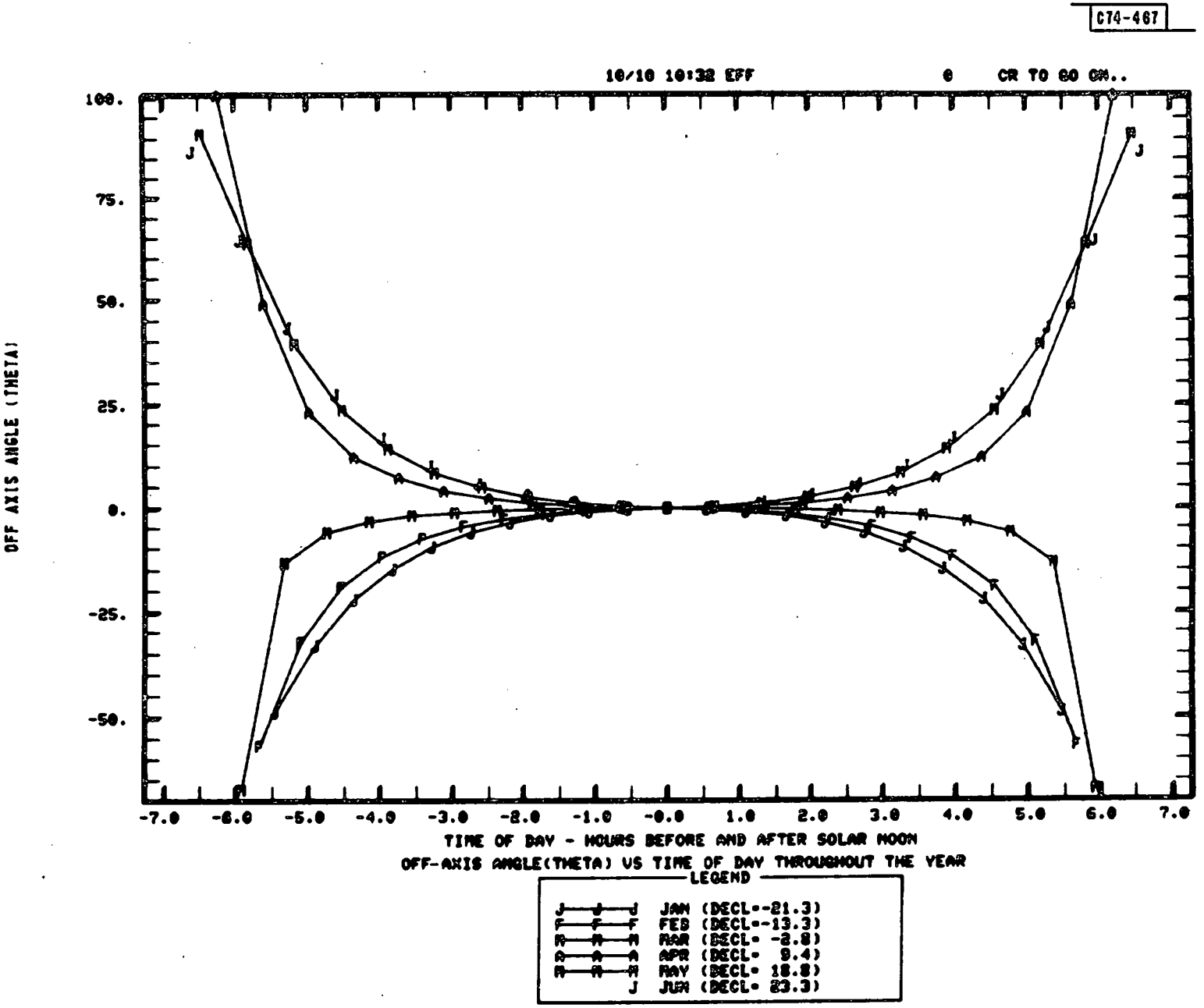

Figure 13 January-June.

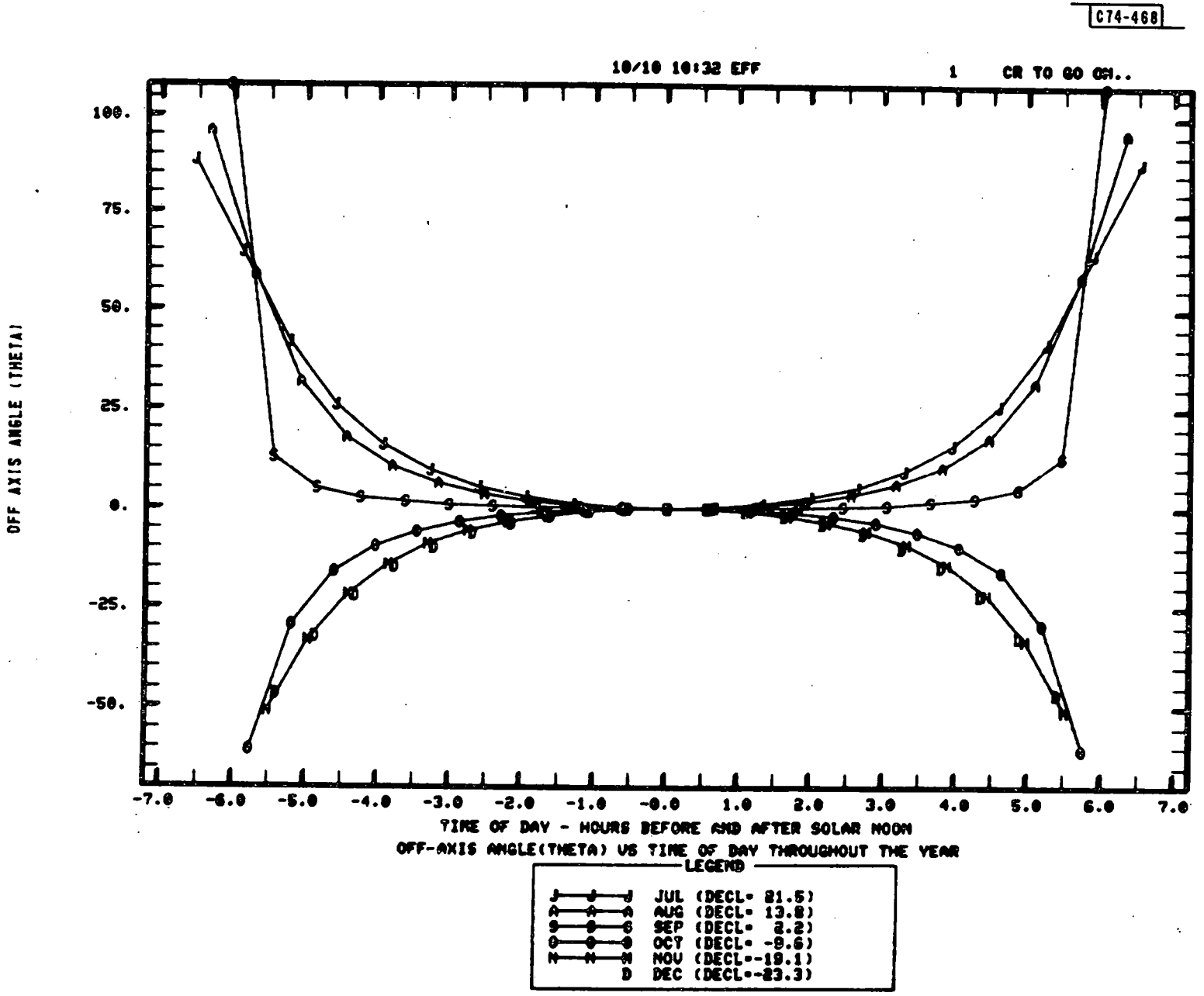

Figure 14 July-December.

trapezoidal trough concentrator's performance is shown in Figure 15. Other types of trough concentrators, such as the compound parabolic concentrator, exhibit similar effects during the summer.

Another problem is that concentrator systems are not able to utilize the diffuse portion of the insolation. In those areas of the world where the skies are mostly clear, the direct component of insolation is large and a concentrator system works efficiently. However, in areas which have long periods of overcast weather, such as the monsoon areas of Orissa, performance is severely degraded.

The performance of a trapezoidal trough concentrator in Orissa is shown in Figure 16. This figure shows the effects both of the off-axis angle between the sun and the collector and of the increase of the diffuse insolation (and consequent decrease in direct insolation) due to clouds. During the summer months, when heavy cloud cover is frequent and the sun's path diverges furthest from the concentrator's axis, the performance of the concentrator array pumping system is essentially zero. The flat-plate-array pumping system, however, will continue to work in this situation.

A third problem associated with reflective concentrators is the loss incurred at the mirrored surface. The best reflectance that can be achieved on a polished (or vapor-deposited) aluminum surface is approximately 88%. In tests this result was only achieved on a microsheet second-surface mirror. Although these mirrors offer excellent optical qualities and excellent long-term stability and durability when mounted on suitable substrate, they are much too costly to use in a practical system. Polished aluminum sheets were also tried, but accelerated aging tests showed that the initial test surface reflectance of 84% degraded to 71% after only 45 days. These test measurements were made using a Gier Dunkle Reflectometer with a Xenon lamp after the panels were subjected to three 15-minute intervals of water spray each day. The weathered samples were etched and clouded. Other tests made on a metalized Mylar-film reflector showed that surface to be unsuitable for a long-life high-quality concentrator.

Additional undesirable effects are a decrease in cell efficiency proportionate to increasing cell temperature (caused by the concentration of the radiant energy) and non-uniform illumination across the cell during those

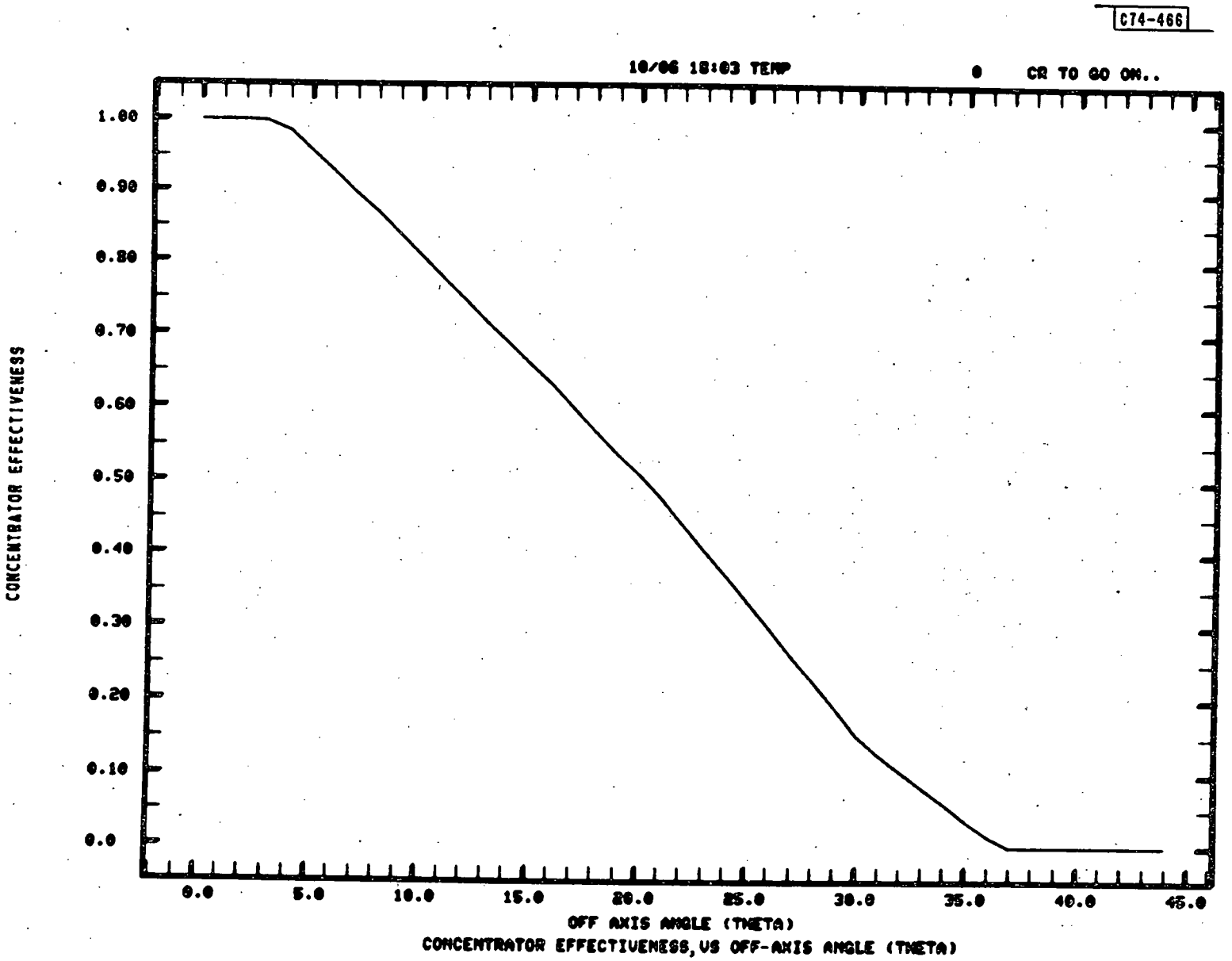
C74-466
10/06 18:03 TEMP
0 CR TO GO ON..
CONCENTRATOR EFFECTIVENESS
1.00
0.90
0.80
0.70
0.60
0.50
0.40
0.30
0.20
0.10
0.0
0.0
5.0
10.0
15.0
20.0
25.0
30.0
35.0
40.0
45.0
OFF AXIS ANGLE (THETA)
CONCENTRATOR EFFECTIVENESS, VS OFF-AXIS ANGLE (THETA)

Figure 15

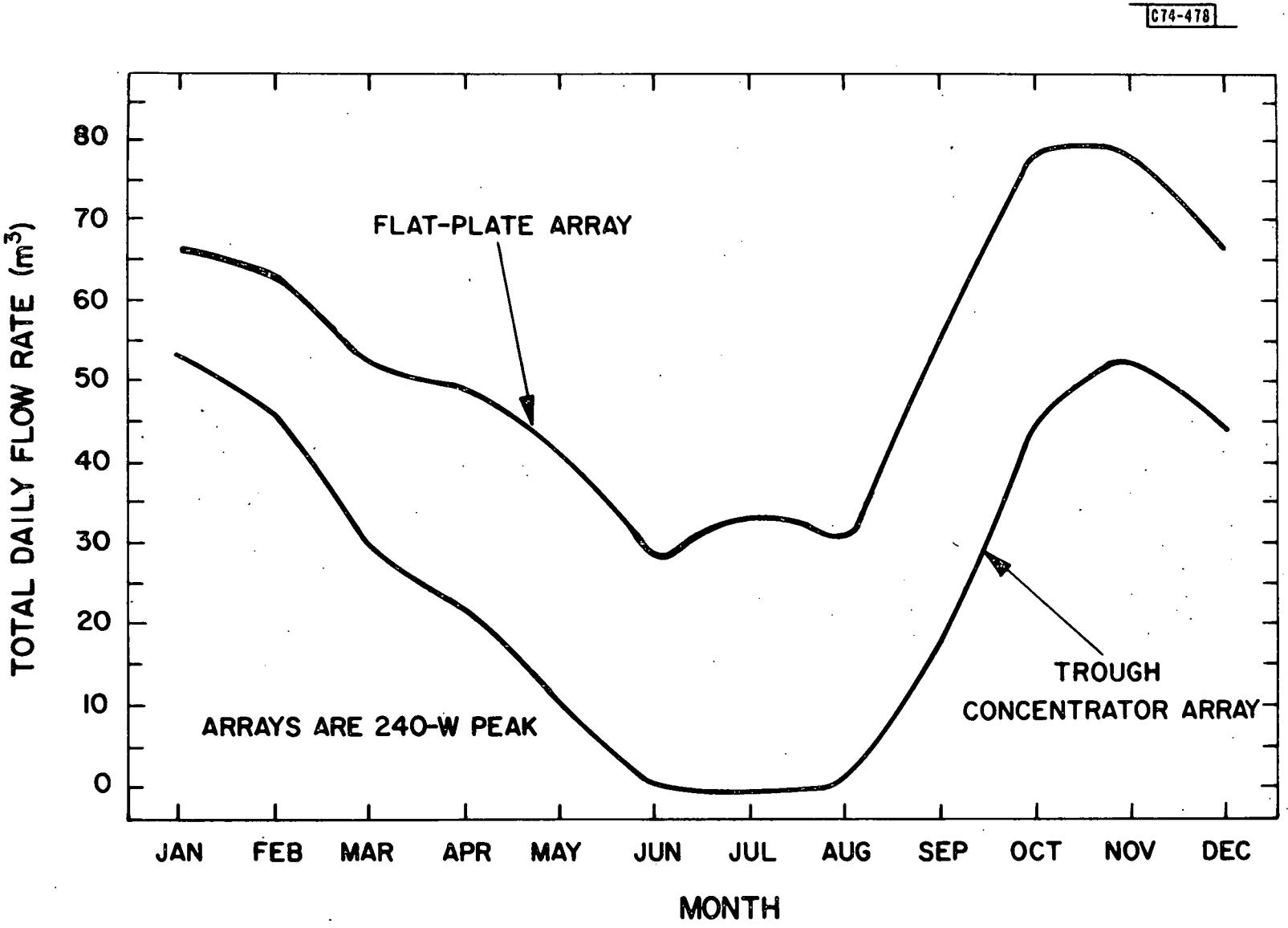

TOTAL DAILY FLOW RATE FOR FLAT-PLATE ARRAY Vs. TROUGH CONCENTRATOR ARRAY FOR ORISSA, INDIA

Figure 16

periods when the sun is not directly along the concentrator's axis. Furthermore, mobile array systems are size limited if they are to be manageable. For a given array size, a concentrating system will produce approximately 15 to 20% less power because of the optical losses at the reflecting surfaces. Finally, when photovoltaic modules reach prices of $2/watt peak and below, the cost advantage of low-concentration collectors will be mostly or entirely lost.

2.5 Systems Including Batteries

The use of batteries is often proposed as a way to increase the overall daily efficiency of a pumping system, the arguments being 1) at high-insolation levels "excess" power from the solar array can be stored for later use when the insolation has decreased, and 2) at low-insolation levels, where the pump is less efficient, energy can be stored and later discharged at a higher-efficiency pumping level. For this particular system, the excess power argument does not apply; the pump, motor and array are so sized that the system can always utilize the total array power. The second argument does apply, however, although performance benefits may not always be as great as one initially might think because of the inefficiencies of the battery system.

The watt-hour efficiency of a battery is defined as the ratio of energy discharged to the energy input required to restore the battery to its original charge state. For a lead-acid battery, this efficiency is about 75%; losses in the attendant battery charger drop the effective battery efficiency to about 70%. Batteries can be connected directly across the array for charging, but elimination of the losses incurred with a charger is more than offset by the fact that the array will seldom be operating at the maximum power point.

The problems encountered at low-insolation levels can be seen in Figure 17, which presents efficiency versus flow rate taken from a typical pump. Data are shown for two heads, 2.6 m and 5.0 m. For the lower head, efficiency maximizes at 30 gpm (120-W motor input) and decreases slightly for higher flow rates. At the higher head, efficiency at 35 gpm (corresponding to maximum-rated array power for 100% insolation) has not quite maximized. Note that in both uses below 20 gpm, efficiency drops off quite rapidly. Thresholds at which pumping begins are 118 W (about 50% insolation) at 5.0-m head and 62 W (about 25% insolation) at 2.6-m head.

Incorporation of a battery would permit intermittent pumping when insolation is below the pumping threshold. The pump would shut down while the battery charged and then operate until the battery discharged to a certain depth or until the insolation level increased. Even on clear, sunny days, a properly designed battery system can improve the volume of water pumped by 10 to 20%.

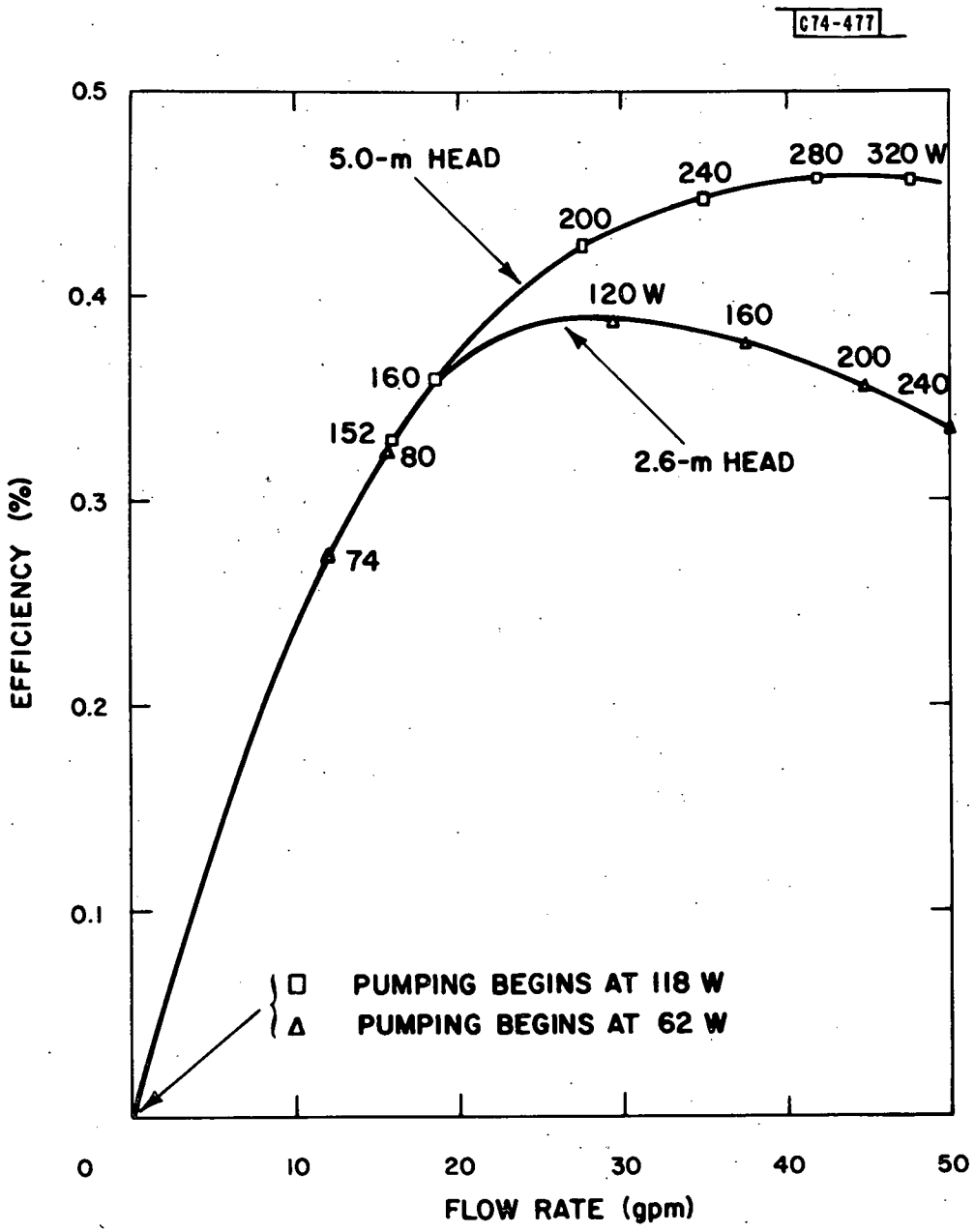

Figure 17 Overall pump set efficiency vs. flow rate.

Use of a battery, however, introduces several problems:

1) Commercial lead-acid batteries store about 10 to 13 watt-hours per pound. A 500 watt-hour battery, capable of pumping for two to four hours before recharging, will add about 50 pounds to the system, (including weight of mounting hardware and control circuitry).
2) Manufacturing costs (and thereby sale price) of the system will be increased.
3) Lead-acid cells tend to lose capacity with repeated charge/discharge cycling. Nickel-cadmium cells are better in this respect and can be reconditioned but are more expensive.
4) Life and reliability of batteries in remote areas may be a problem. ("Return to your local dealer for warranty exchange" may not be feasible.) Standard lead-acid battery cells require periodic replenishment with water which preferably is distilled but at least is reasonably pure. Maintenance-free lead-acid batteries have recently appeared on the market, but battery life (judged on the basis of warranties) is shorter for these batteries than for those which require maintenance.
5) Batteries must be protected against excessive discharge and overcharge, which requires monitoring and control circuitry.

In the light of these problems, it was decided to design the system without a battery, despite possible operating performance improvements that a battery might yield. Presently available insolation data are inadequate to determine whether the pump system will operate at projected daily efficiencies all year long in all proposed locations, but indications are that satisfactory and useful operations would occur most of the year in most locations.

3.0 SYSTEM PERFORMANCE

The performance of the prototype PV-powered pumping system was predicted by using a computer simulation. Each of the system elements was modeled in order to determine the overall performance algorithm. The equations of motion of the sun as a function of time of day, time of year, and latitude were added along with provisions for monthly input of the water-table level, the ambient temperature and the total daily horizontal insolation. The array and motor/pump set characteristics were then added and the performance of the prototype microirrigation system determined for two locations. These locations were Orissa, India, representative of a monsoon weather region; and Cairo, Egypt, an area with excellent year-round sunlight. The results of these simulations are shown in Figures 18 and 19.

The computer program progresses from input to final system performance along the flow path shown in Figure 20. First, an hourly insolation profile for a typical day is generated for each month of the year based on the total daily horizontal insolation for the location specified. This profile includes the analytical separation of the insolation into its "direct" and "diffuse" components. This insolation, the maximum available to an array positioned normal to the incident solar rays, is then modified to account for the actual position of the array at any given time. This allows for the incorporation of tracking, partially tracking and non-tracking arrays into the simulation.

Next, the available array output, expressed as a current-voltage (I-V) characteristic, is generated for each value of hourly insolation. The array output is determined by the equation:

$$I = I^*_{sc}\left(\frac{L}{L^*} - 1\right) + \alpha(T-T^*) + I^*_{sc}\left\{1-e^{\left[\left(\frac{k}{V_{oc}}[V+\beta(T-T^*)]\right) - k\right]}\right\}$$

where: ( )* = parameters with module at standard conditions ($100 mW/cm^2$ and 28°C)

I_{sc} = short-circuit current

V_{oc} = open-circuit voltage

L = insolation

T = cell temperature

k, α, β = constants.

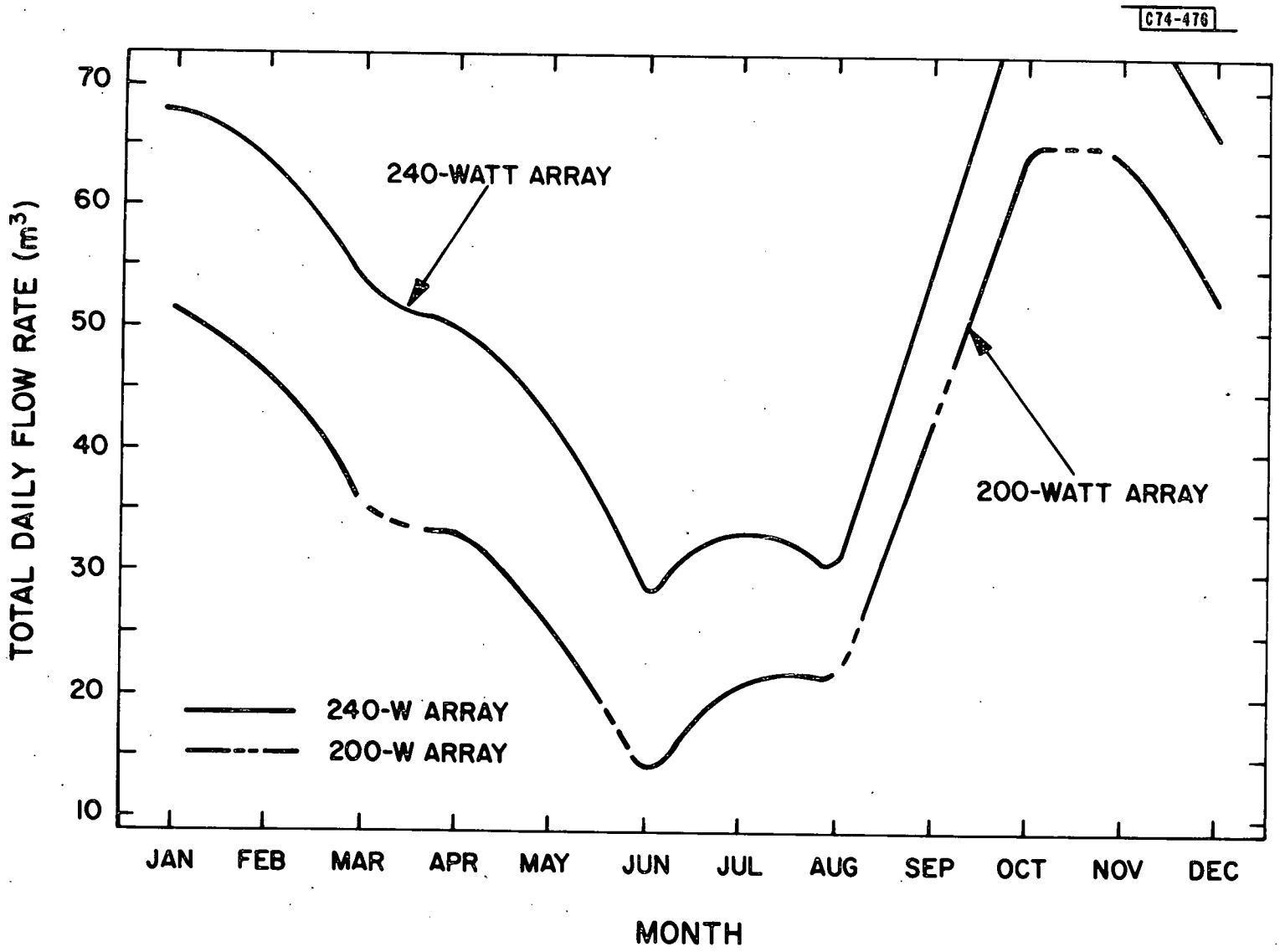

TOTAL DAILY FLOW RATE Vs. MONTH FOR ORISSA, INDIA

Figure 18

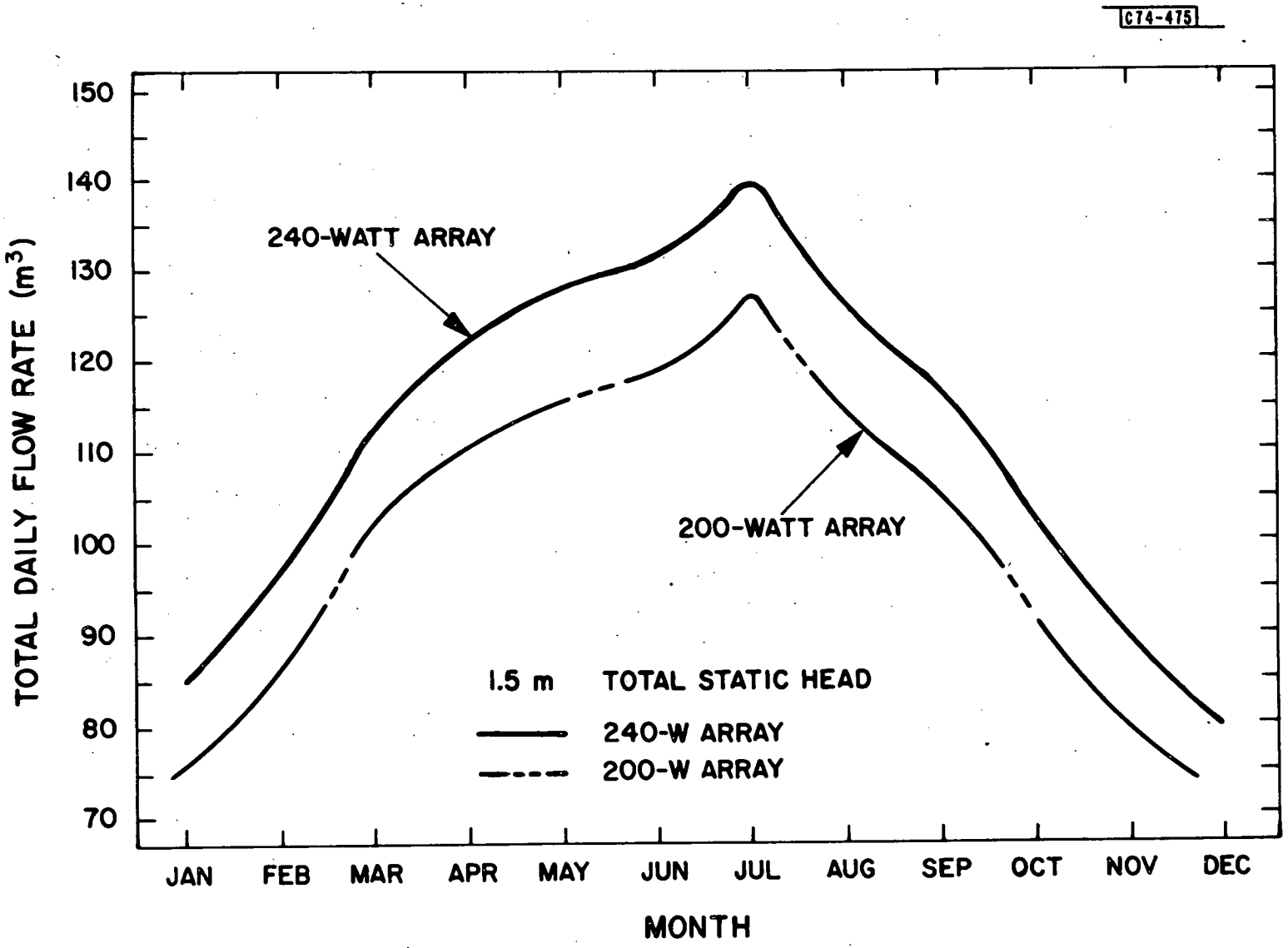

TOTAL DAILY FLOW RATE Vs. MONTH FOR CAIRO, EGYPT

Figure 19

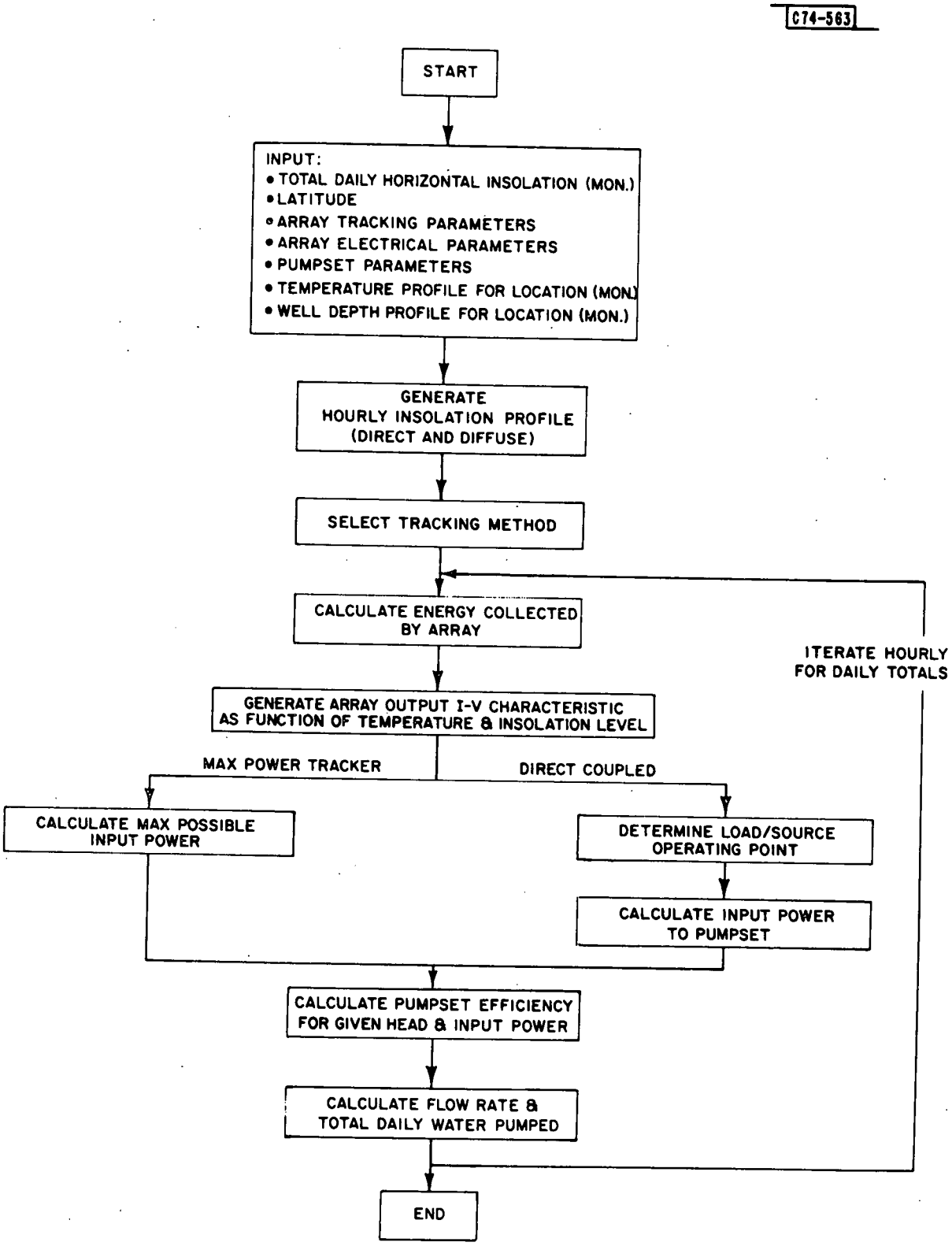

Figure 20 Computer flow path.

This equation accounts for cell-temperature effects as well as varying insolation effects. The temperature used in the formula is cell temperature and not ambient temperature. The cell temperature was assumed to be:

$$T = \tilde{T} + C\left(\frac{L}{L^*}\right)$$

where: $\tilde{T}$ = ambient temperature (°C)

C = 25°C.

For the case where a maximum-power-point tracker is utilized in the system, the current and voltage values corresponding to the maximum possible power generated are determined and 95% of the power is transmitted to the motor/pump combination. The remaining 5% is lost as heat in the maximum-power-point tracker. Finally, the flow is calculated by conversion of the electrical energy into mechanical energy corrected by the motor/pump efficiency for the given conditions of head and flow. This is represented by the equation:

$$F = \frac{c\ P\ E_{ff}}{H}$$

where: F = flow

H = head

P = power

c = constant

E_{ff} = efficiency characteristic of motor/pump set and is a function of F and H.

The representation of E_{ff} is an analytical approximation of actual test data for a given motor/pump set. A close representation in the regions of interest in this simulation is:

$$E_{ff} = \phi(H^2)\ \psi(F^2)$$

where: $\phi(H^2)$ represents a function which is second order with respect to H

$\psi(F^2)$ represents a function which is second order with respect to F.

For the case where a maximum-power-point tracker is not used, an equivalent I-V curve for the pump/motor set is determined from test data. This represents the "load" I-V curve. For the units tested, this curve was approximated by the form:

$$I_{load} = k_1 V_{load}^{k_2} - k_3$$

where: k_1 = function (H^3)

k_2 = constant

k_3 = function (H^3).

The intersection of the load line and the module I-V curve is determined to find the motor/pump set operating point. The flow can now be determined readily by calculating the available power and continuing as described above.

Lastly, the accumulated daily flow is determined by integration of the varying flow during the day.

Several examples of the results from the simulation are presented. Figure 18 shows the daily predicted total flow for the micropump prototype unit in Orissa, India. The water-table depth and ambient-temperature values by month that were used to generate this figure are shown in Figures 21 and 22. Orissa, India, is typical of areas with monsoon weather patterns.

Figure 19 shows the predicted total flow for the micropump prototype unit in Cairo, Egypt. Cairo does not have a monsoon weather pattern, and hence shows that much greater flows are possible during its dry summer growing season.

Figures 18 and 19 are for flat, twice-daily adjusted panels. Figures 23 and 24 show flows from similar conditions, except that trough concentrator collectors are used. The performance of these collectors has been calculated; it includes the effects of off-axis misalignment between the sun and the trough major axis and accounts for the fact that only direct insolation can be focused. As is seen in Figure 23, the long periods of overcast weather preceding and during the monsoon make a concentrator-based system unattractive in the monsoon area of Orissa, India.

C74-471

ORISSA
TYPICAL WATER-TABLE DEPTHS IN LOWLAND WELLS*
(Meters Below Ground Level)

DISTRICT	JAN	FEB	MAR	APR	MAY	JUN	JUL	AUG	SEP	OCT	NOV	DEC
1. KORAPUT	1.6	1.9	2.5	3.9	3.9	4.5	0.5	0.2	0.3	0.4	1.0	1.2
2. PHULBANI	4.5	5.8	8.0	5.5	5.0	4.5	6.5	5.5	4.5	3.5	3.5	3.8
3. BALASORE	2.8	4.1	4.3	4.6	4.9	5.0	4.8	4.5	3.5	2.5	2.8	3.4
4. CUTTACK	2.0	1.6	1.4	1.4	1.4	1.7	1.6	1.0	1.2	1.2	1.3	1.6
5. GANJAM	2.7	2.9	3.0	3.0	2.5	2.5	3.0	3.0	2.5	1.0	1.1	1.8
6. KEONJHAR	2.0	2.0	2.0	2.1	2.2	2.2	2.0	1.5	1.2	1.0	2.0	2.0
7. PURI	2.5	3.0	3.5	3.9	4.3	4.5	2.0	1.3	1.4	1.3	1.7	2.1
"AVERAGE" OR TYPICAL	2.6	3.0	3.5	3.5	3.5	3.6	2.9	2.4	2.1	1.6	1.9	2.3

*Source: OLIC Hydrologic Records, '74-'75

Figure 21

C74-472

ORISSA
MONTHLY AVERAGE TEMPERATURES IN DIFFERENT DISTRICTS (°F)

DISTRICT	JAN	FEB	MAR	APR	MAY	JUN	JUL	AUG	SEP	OCT	NOV	DEC
1. KORAPUT	66	76	84	89	91	85	80	80	79	78	73	69
2. PHULBANI	62	70	77	82	83	82	81	80	80	79	70	63
3. BALASORE	69	74	79	88	93	90	88	87	86	84	77	69
4. CUTTACK	65	73	80	83	84	82	85	85	85	83	75	69
5. GANJAM	61	70	78	88	89	87	84	81	78	77	71	65
6. KEONJHAR	67	71	83	88	90	88	84	84	83	81	75	69
7. PURI	68	78	85	88	90	95	88	87	86	84	75	69
"AVERAGE" OR TYPICAL	65	73	81	87	89	87	84	83	82	81	74	67

Figure 22

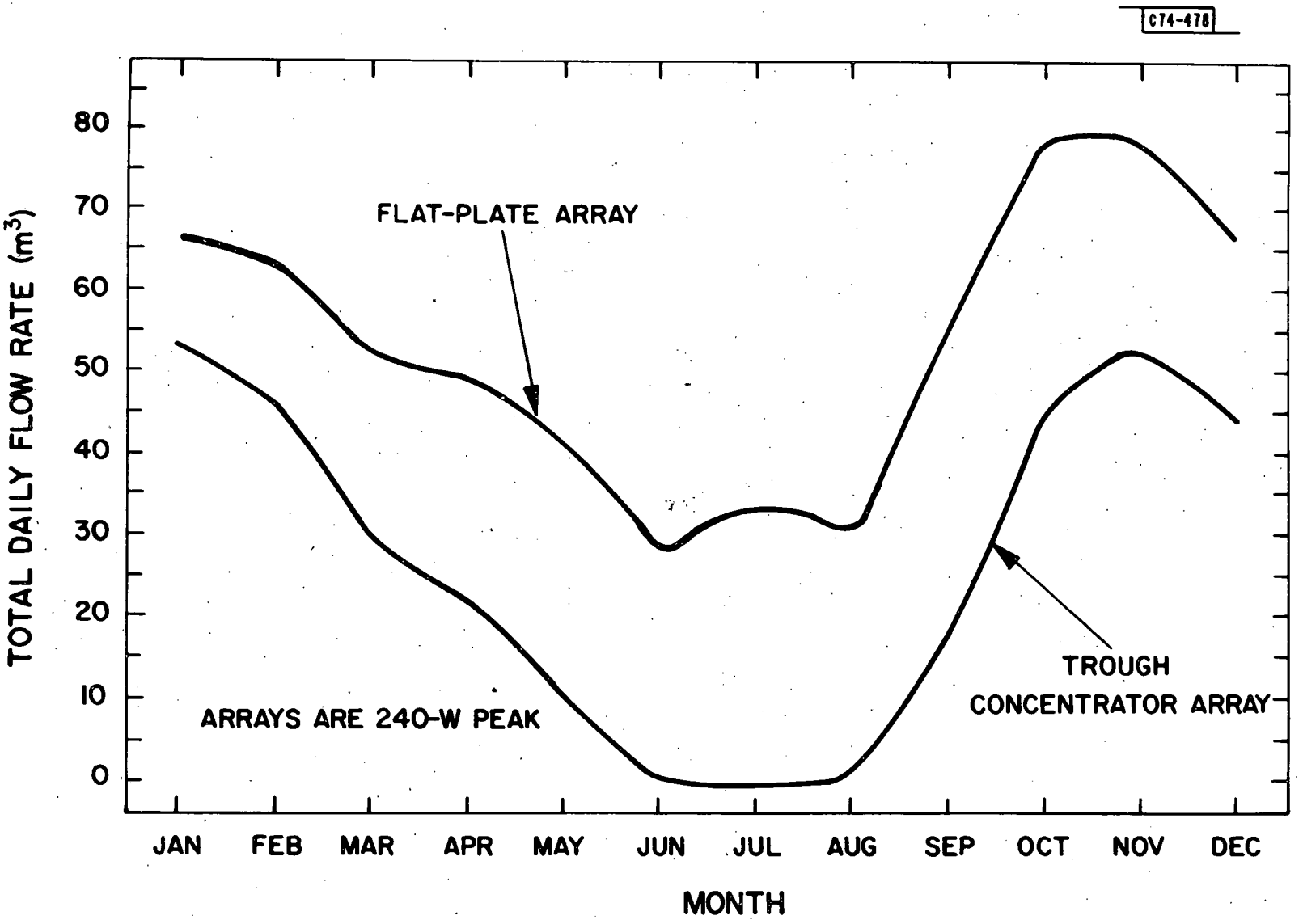

TOTAL DAILY FLOW RATE FOR FLAT-PLATE ARRAY Vs. TROUGH CONCENTRATOR ARRAY FOR ORISSA, INDIA

Figure 23

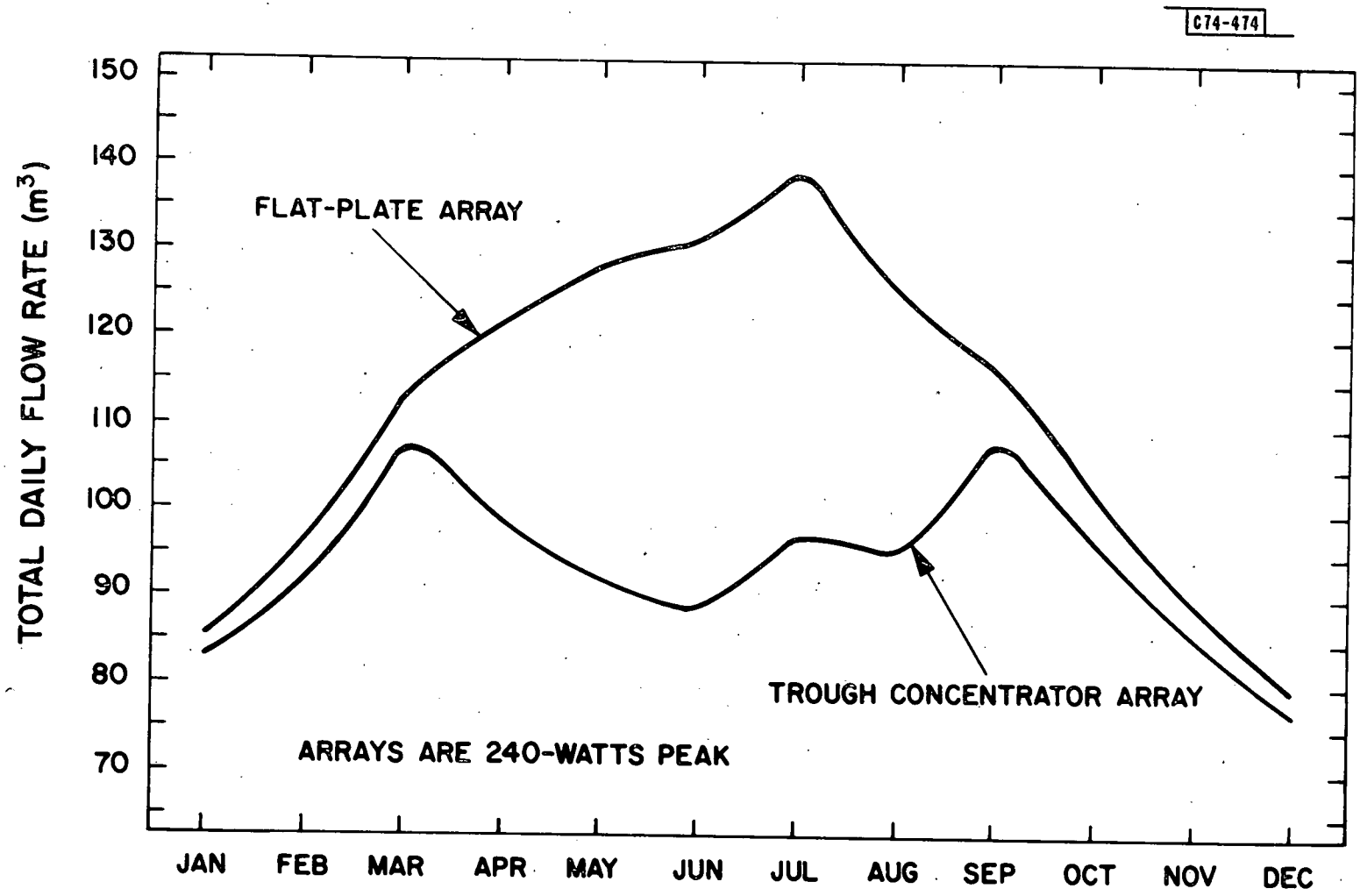

TOTAL DAILY FLOW RATE FOR
FLAT-PLATE ARRAY Vs. TROUGH CONCENTRATOR ARRAY
CAIRO, EGYPT

Figure 24

4.0 PROTOTYPE SYSTEM DEVELOPMENT & DESCRIPTION

Concurrent with the analyses described in the previous sections, an effort was made to actually develop and test a prototype unit. A target wire-to-water efficiency of 50% was selected for the development under conditions of 40 gallons/minute at a maximum head of 5 meters. After tests of many different pumps and motors and combinations thereof, a maximum efficiency of 47% was achieved. This system is shown in Figure 1, with additional views of the components in Figures 25, 26 and 27.

A search was made for a permanent magnet 1/4-1/3-hp DC motor of the highest efficiency commercially available. Based on manufacturers' product specifications and discussions with manufacturers, three motors were selected, purchased and tested. The motors were made by Mavilor, Indiana General and Applied Motors. The latter two were approximately equal, with each achieving nearly 85% efficiency in changing electrical energy into mechanical energy. It was evident, however, that two modifications would have to be made in order to use either motor in the prototype unit. Of greatest importance was the need to protect the motor from water by building a submersible housing around it; a graphite/chrome surface face seal was placed about the rotating motor shaft connected to a sealed aluminum cannister encasing the rest of the motor. The second modification concerned the motor voltage/speed characteristics. The motors that were available as standard commercial components were wired to provide 1800 rpm at 90 volts. The desired parameters for the Sun Pump were 3000 rpm at 65 volts. Therefore, several specially wound motors were ordered and it is these which are described in this paper.

A search was also made for the commercially available pump of the highest efficiency for use at the flow rate and head indicated above; letters were sent to hundreds of manufacturers and dozens of phone calls were made. In general, pumps in this size range are designed for low cost rather than high efficiency. However, a couple of units were found that exhibited reasonable efficiency ($\sim$ 60%)--a Deming centrifugal pump and a Demster Industries vertical turbine (single stage of a multistage unit) pump. These pumps are quite close to the expected upper bound of efficiency for available pumps as shown in Figure 5.

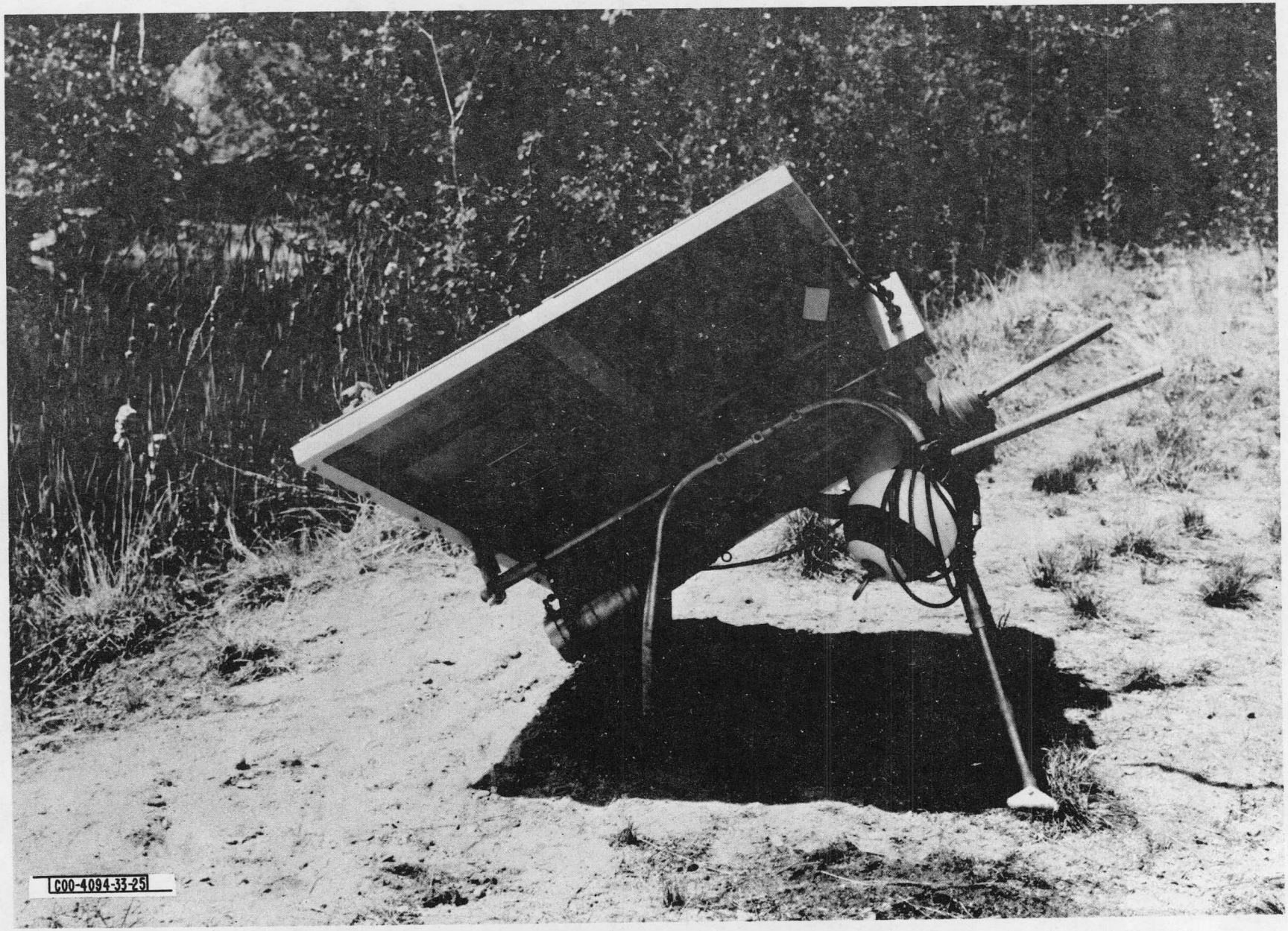

Figure 25 Prototype micropump - stored condition.

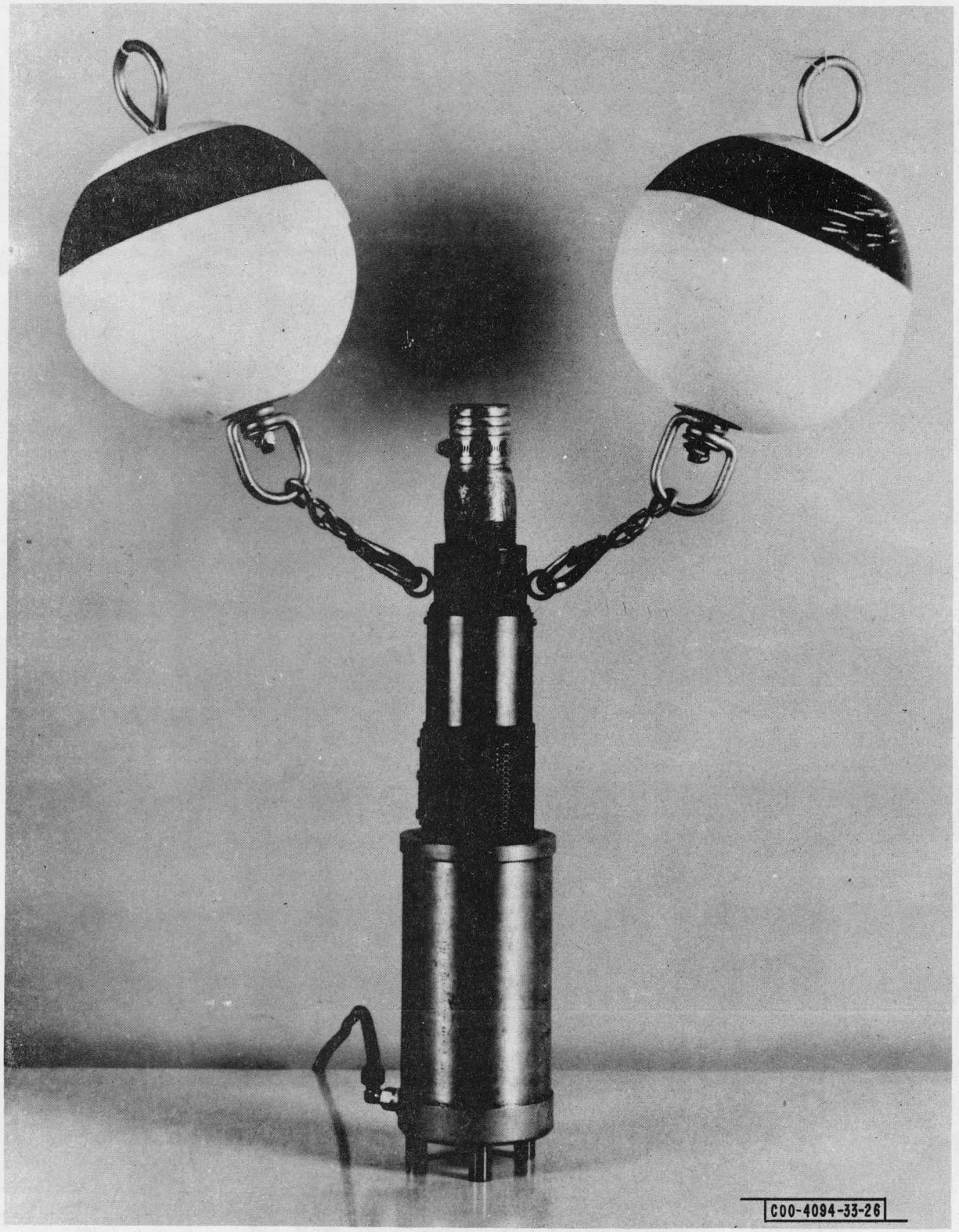

Figure 26 Submersible pump set.

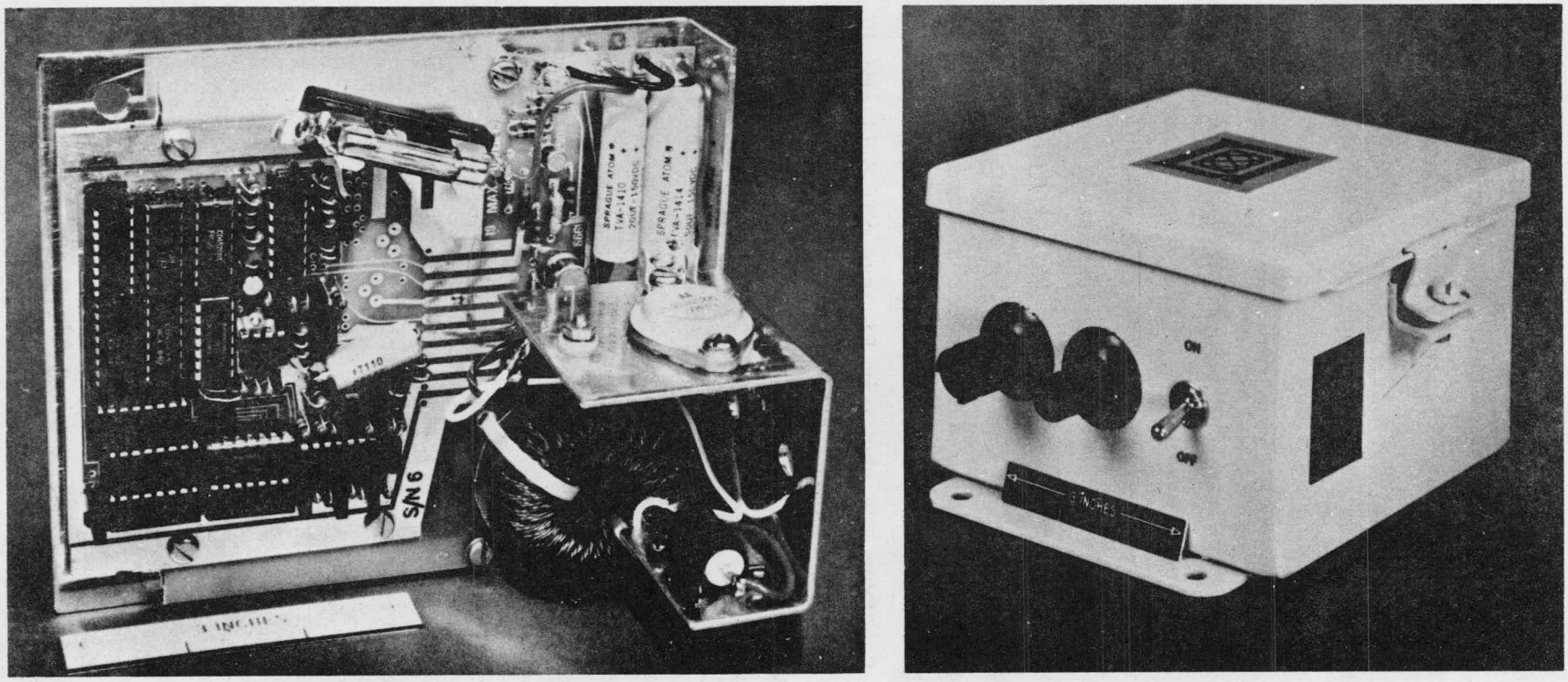

Figure 27 Maximum-power-point tracker.

At the operating conditions desired (40 gpm at 5 meters and 3000 rpm) the pump is operating at a specific speed of 2300. This corresponds (from Figure 5) to an achievable efficiency of 63%. The two pumps mentioned above are a little below this and hence could be somewhat improved. In any case, the vertical turbine pump was selected for the prototype as it had the versatility of being usable in a tube well as well as a dug well.

The test setups to measure the motor characteristics and the pump/motor set combined characteristics are shown in Figures 28 and 29. In Figure 28 a dynamometor was made to determine the output torque and speed (with a strobascope) as a function of input power at different voltage levels. Figure 29 shows the pumping facility that was used to determine the wire-to-water efficiency. The flow rate was monitored, along with the height pumped and head as measured with a pressure gage, allowing the output power to be calculated. The input power was determined by a voltmeter and ammeter connected to the input terminals of the motor. The characteristics of the final configuration of the micropump prototype are shown in Figures 6,7,8,11 and 17. As can be seen, the pump is near the target 50% (actual maximum efficiency achieved was 47%) at the nominal operating conditions. However, the efficiency drops off at lower heads. At a 1 1/2-meter head, a typical value for lifting water from a canal, the efficiency has degraded dramatically although the actual water pumped has increased. This is caused by the shifting of the specific speed from 2300 at 5 meters to nearly 8000 at 1 1/2 meters. The internal configuration of a pump designed for operating efficiently at a specific speed of 8000 would be different from that for 2300. Hence a different pump, one more closely resembling an axial-flow configuration, would be desired to optimize the flow for the canal-lift situation. However, at the 5-meter lift the prototype unit performed as was desired.

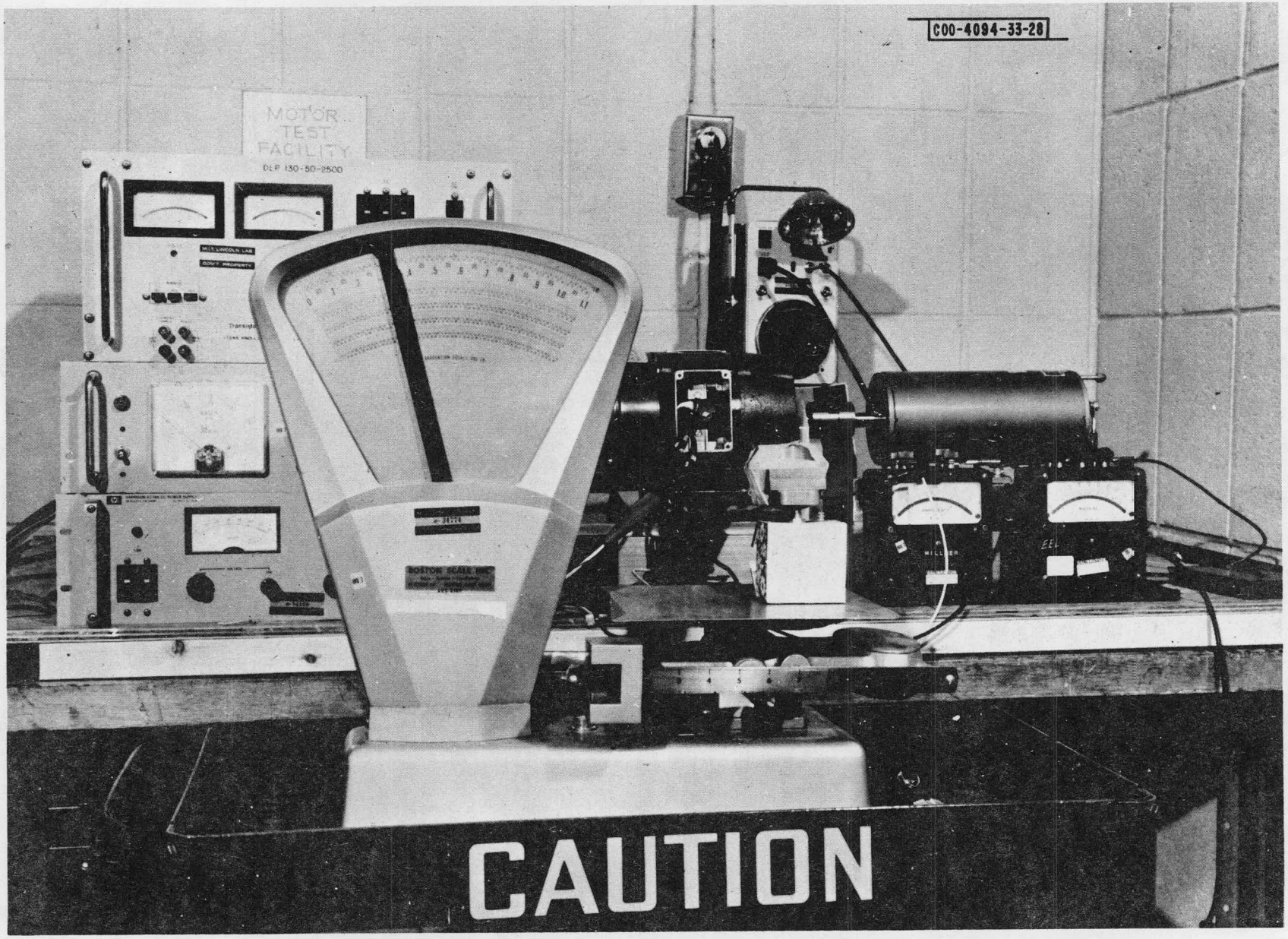

Figure 28 Motor test apparatus.

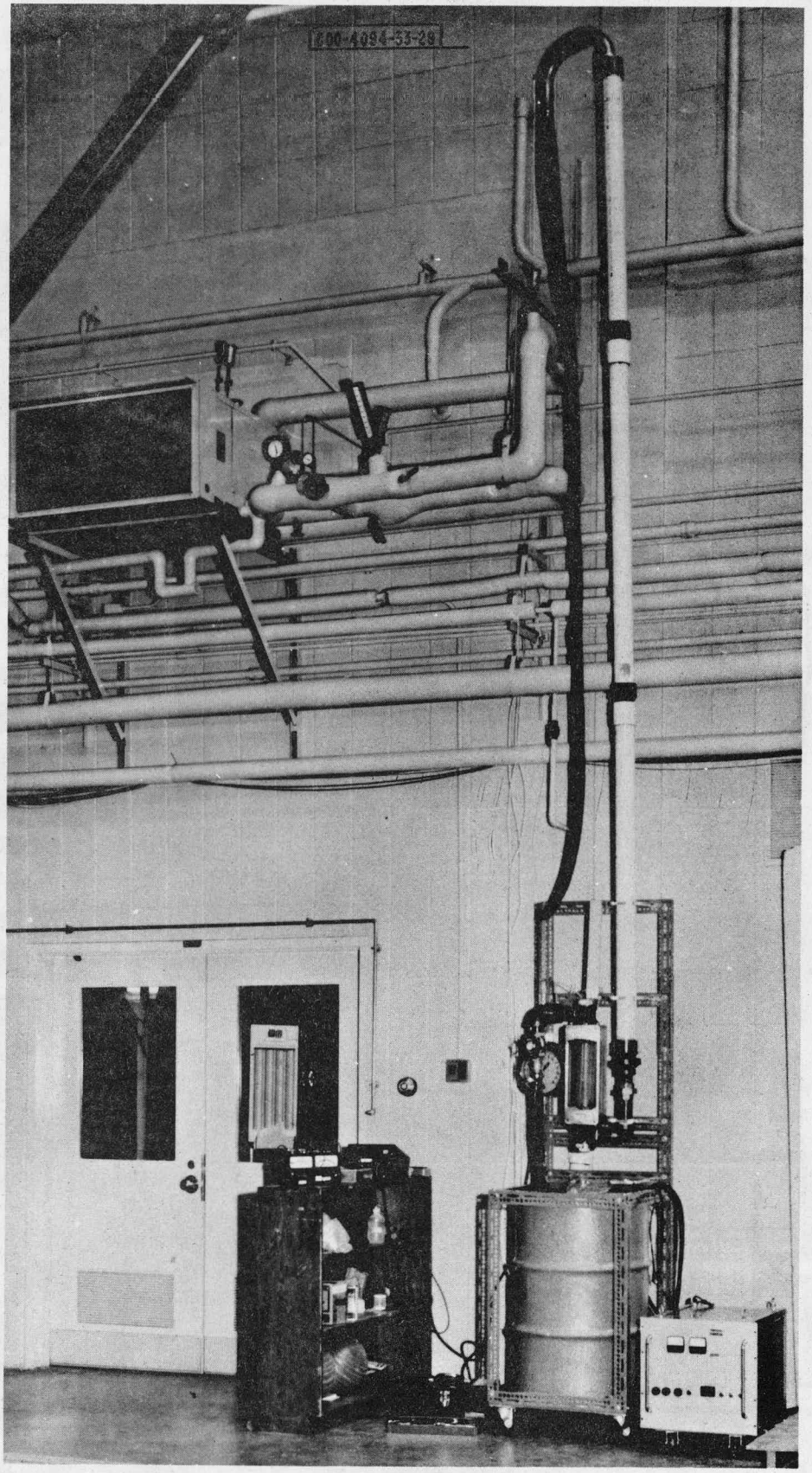

Figure 29 Pump set test apparatus.

Bibliography

1. Smith, D. V., "Photovoltaic Power in Less Developed Countries," MIT/Lincoln Laboratory, Lexington, MA, COO/4094-1, 24 March 1977.

2. Allison, S.V., and Smith, D.V., "Microirrigation with Photovoltaics," MIT/Energy Laboratory, Cambridge, MA, MIT-EL-78-006, April 1978.

3. Tabors, R.D., "The Economics of Water Lifting for Small-Scale Irrigation in the Third World: Traditional and Photovoltaic Technologies," MIT/Energy Laboratory, Cambridge, MA, MIT-EL-78-015, August 1978.

4. Roger, J.A., et al., "Calculations and In Situ Experimental Data on a Water Pumping System Directly Connected to a 1/2 kW Photovoltaic Converter Array," presented at 1977 Photovoltaic Solar Energy Conference, Luxembourg, 27-30 September 1977.

5. Prido, R., "Water Pumping System Using Solar Power from Photovoltaic Source," presented at 1977 Photovoltaic Solar Energy Conference, Luxembourg, 27-30 September 1977.

6. Durand, H., and Naaijer, G.J., "Water Pumps Driven by Photovoltaic Modules," Heliotechnique and Development, pp.315-330.

7. Meinel, M.P., "Solar Energy Applications to Water Pumping and Agriculture," Heliotechnique and Development, pp.307-314.

8. Landsman, E.E., "Maximum Power Trackers for Photovoltaic Arrays," 1978 IEEE PV Specialists' Conference, Washington, D.C., 5-8 June 1978.

9. Karassik, I.J., et al., "Pump Handbook," McGraw-Hill Book Company, New York, 1976.

10. Pillai, K.P.R., "A Survey of Pumps," Chemical Age of India, Vol. 20, No. 5, May 1969, pp.349-395.

11. Rost, M., and Visich, E.T., "Pumps," Chemical Engineering - Deskbook Issue, 14 April 1969, pp.45-57.

12. deJong, B., "Net Radiation Received by a Horizontal Surface at the Earth," Delft University Press, 1973.

Acknowledgments

The author expresses his appreciation to B. Grossman for her help in programming the computer simulation and to J. Husler for his help with the mechanical design, fabrication and testing of the prototype unit.

APPENDIX

Source and Load Power Maximizing Criteria (See Section 2.3)

Source Maximization

Consider a monotonic source characteristic $I = f(V)$ as shown in Figure A1. Power delivered by this source at any point can be represented by:

$$P = VI = Vf(V). \tag{A1}$$

To determine the condition for maximum power, we set $\frac{dP}{dV} = 0$, which leads to

$$Vf'(V) = -f(V). \tag{A2}$$

Substituting I and $\frac{dI}{dV}$, respectively, for $f(V)$ and $f'(V)$ yields:

$$\frac{dI}{dV} = -\frac{I}{V} \tag{A3}$$

which is the condition for maximum source power. Note that the source can be double-valued in V or I or both as long as the monotonic criterion is met.

Examination of Figure A-1 shows a simple technique for graphically determining the maximum power point of a source I-V characteristic. One constructs by trial and error the isoceles triangle for which the apex lies on the source I-V curve and the side drawn from $2V_{pmax}$ (or $2I_{pmax}$) is tangential to the source I-V curve.

Load Maximization

In Figure A-2, we see three different load I-V curves, with a common assumed operating point (I_L, V_L). Load 1 is single-valued in voltage and current and has positive slope everywhere. Load 2 is single-valued in voltage only, while Load 3 is single-valued in current only. (Note the load characteristic having a multi-valued variable automatically implies negative incremental resistance or conductance in some region.)

Power delivered to the load is:

$$P = V_L I_L. \tag{A4}$$

Let us vary V_L and require that the corresponding change in power be ≥ 0; i.e.,

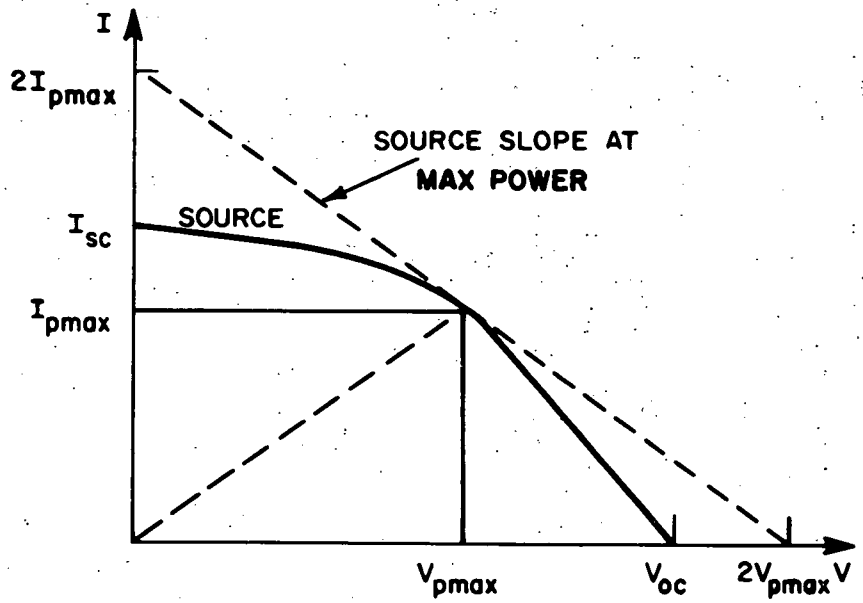

Figure A1 Power maximization at source.

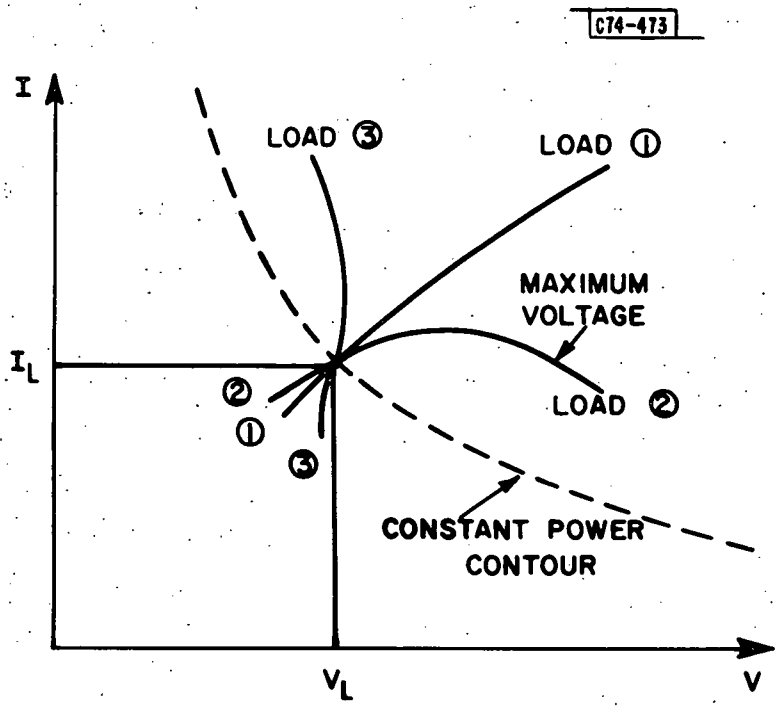

Figure A2 Power maximization at load.

$$\delta P = \frac{dP}{dV_L}\,\delta V_L = \left(I_L + V_L \frac{dI_L}{dV_L}\right)\delta V_L \geq 0 . \tag{A5}$$

Now if $\delta V_L > 0$, $\quad V_L \frac{dI_L}{dV_L} \geq - I_L$ or $\frac{dI_L}{dV_L} \geq - \frac{I_L}{V_L}$ (A6)

while if $\delta V_L < 0$, $\quad - V_L \frac{dI_L}{dV_L} \geq I_L$ or $\frac{dI_L}{dV_L} \leq - \frac{I_L}{V_L}$. (A7)

Note that these conditions can be applied to Loads 1 and 2 but break down for Load 3 because of the occurrence of $\frac{dI_L}{dV_L} = \pm \infty$ on the latter.

In a similar manner, by varying I_L, if $\delta I_L > 0$,

$$\frac{dV_L}{dI_L} \geq - \frac{V_L}{I_L} \tag{A8}$$

while if $\delta I_L < 0$, $\quad \frac{dV_L}{dI_L} \leq - \frac{V_L}{I_L}$ (A9)

and these conditions can be applied to Loads 1 and 3, but not to Load 2.

Hence, to increase or maximize power into a load, one must control via a single-valued variable. Note that if a load which has a maximum power point, operation at that point implies equality in Eqs. (A6) through (A9) which in turn leads to the same criteria as source maximization, i.e.,

$$\frac{dI}{dV} = - \frac{I}{V} .$$